General Disclaimer

One or more of the Following Statements may affect this Document

- This document has been reproduced from the best copy furnished by the organizational source. It is being released in the interest of making available as much information as possible.

- This document may contain data, which exceeds the sheet parameters. It was furnished in this condition by the organizational source and is the best copy available.

- This document may contain tone-on-tone or color graphs, charts and/or pictures, which have been reproduced in black and white.

- This document is paginated as submitted by the original source.

- Portions of this document are not fully legible due to the historical nature of some of the material. However, it is the best reproduction available from the original submission.

THE EFFECTS OF AIRCRAFT DESIGN ON STOL RIDE QUALITY

Technical Report

Grant No. NGR 47-005-208

Submitted to:

National Aeronautics and Space Administration
Scientific and Technical Information Facility
P.O. Box 8757
Baltimore/Washington International Airport
Baltimore, Maryland 21240

Submitted by:

Craig R. Jones

and

Ira D. Jacobson

SCHOOL OF ENGINEERING AND APPLIED SCIENCE

RESEARCH LABORATORIES FOR THE ENGINEERING SCIENCES

UNIVERSITY OF VIRGINIA

CHARLOTTESVILLE, VIRGINIA 22901

Report No. ESS-4035-103-75

May 1975

THE EFFECTS OF AIRCRAFT DESIGN ON STOL RIDE QUALITY

Technical Report
Grant No. NGR 47-005-208

Submitted to:
National Aeronautics and Space Administration
Scientific and Technical Information Facility
P.O. Box 8757
Baltimore/Washington International Airport
Baltimore, Maryland 21240

Submitted by:
Craig R. Jones
and
Ira D. Jacobson

DEPARTMENT OF ENGINEERING SCIENCE AND SYSTEMS
SCHOOL OF ENGINEERING AND APPLIED SCIENCE
UNIVERSITY OF VIRGINIA
CHARLOTTESVILLE, VIRGINIA

Report No. ESS-4035-103-75
May 1975

ABSTRACT

Effects of aircraft dynamic characteristics on passenger ride quality are investigated to determine ride-quality isocontours similar to aircraft handling-qualities contours. Measurements are made on a moving-base simulator while varying the aircraft short-period and Dutch Roll frequencies and dampings. Both pilot ratings and subjective ride-quality ratings are obtained during "flight." Ride and handling qualities were found to be complimentary for the Dutch Roll mode, but not for the short-period mode. Regions of optimal ride and handling qualities are defined for the short-period mode, and the effects of turbulence levels studied.

TABLE OF CONTENTS

LIST OF TABLES

LIST OF FIGURES

LIST OF FIGURES (Continued)

NOMENCLATURE

a_x, a_y, a_z	accelerations in the x,y,z directions
b	reference length, span
C_D	drag coefficient ($C_D = D/q_\infty S$)
C_L	lift coefficient ($C_L = L/q_\infty S$)
C_ℓ	rolling moment coefficient ($C_\ell = L/q_\infty Sb$)
C_m	pitching moment coefficient ($C_m = M/q_\infty S\bar{c}$)
C_n	yawing moment coefficient ($C_n = N/q_\infty Sb$)
C_y	side force coefficient ($C_y = Y/q_\infty S$)
C_{i_j}	stability derivative ($C_{i_j} = \partial C_i/\partial j$)
$C_{\frac{1}{2}_d}$	number of cycles to half amplitude of the Dutch Roll mode
$\bar{c}$	reference length, MAC
D	drag force
g	acceleration of gravity
h	flight altitude above mean sea level
h*	center of gravity location, fraction of MAC measured from wing leading edge
I_x, I_y, I_z	moments of inertia in body axes
I_{xz}	product of inertia in body axes
L	lift force
L_i	turbulence scale length in the i direction
ℓ, m, n	perturbation from equilibrium L,M,N moments
L,M,N	moments about the x,y,z axes
m	mass (m = W/g)
P,Q,R	angular rates about the x,y,z axes

NOMENCLATURE (Continued)

p,q,r	perturbation from equilibrium P,Q,R angular rates
q_∞	dynamic pressure ($q_\infty = \frac{1}{2}\rho U_0^2$)
S	reference area
$T_{\frac{1}{2}_d}$	time to half amplitude of the Dutch Roll mode
U,V,W	velocity components in the x,y,z axes
U_0	equilibrium flight speed
u,v,w	perturbations from equilibrium U,V,W velocities
$'u$	nondimensional perturbation in U ($'u = u/U_0$)
W	weight
$\bar{w}_g$	gust magnitude
X,Y,Z	forces in the x,y,z directions
x,y,z	conventional right-handed body fixed reference axes
α	angle of attack ($\alpha = w/U_0$)
$'\alpha$	perturbation from equilibrium angle of attack
β	angle of sideslip ($\beta = v/U_0$)
δ_a	perturbation from equilibrium aileron position
δ_e	perturbation from equilibrium elevator position
δ_r	perturbation from equilibrium rudder position
δ_T	perturbation from equilibrium throttle position
ζ_s	damping ratio of the short-period mode
ζ_d	damping ratio of the Dutch Roll mode
Θ	equilibrium pitch angle
θ	perturbation pitch angle from equilibrium

NOMENCLATURE (Continued)

ρ	air density
σ_i	rms gust intensity in the i direction
Φ	equilibrium roll angle
ϕ	perturbation roll angle from equilibrium
ϕ_i	power spectral density in the i direction
$\lvert\phi/v_e\rvert_d$	roll-to-sideslip parameter of the Dutch Roll mode
$\lvert\phi/\beta\rvert_d$	roll-to-sideslip ratio of the Dutch Roll mode
Ψ	equilibrium yaw angle
ψ	perturbation yaw angle from equilibrium
ω	frequency
ω_{n_d}	undamped natural frequency of the Dutch Roll mode
ω_{n_s}	undamped natural frequency of the short-period mode
$(\dot{})$	derivative with respect to time ($(\dot{}) = d(\ )/dt$)
$(\ddot{})$	second derivative with respect to time ($(\ddot{}) = d^2(\ )/dt^2$)

CHAPTER I

INTRODUCTION AND PROGRAM DESCRIPTION

Up until the present time, there have been two completely separate and independent efforts to analyze and improve the ride quality and handling qualities of aircraft. The subject of this dissertation is to define, in a quantitative way, the relationships between these two quantities and to determine what trade-offs exist between the two. This is accomplished by varying the dynamic characteristics of a simulated aircraft in a motion-based simulator and obtaining simultaneous measurements of ride qualities from test passengers riding aboard the simulator and handling qualities from a pilot flying the simulator. Predicted levels of ride quality are also computed using comfort models developed by the University of Virginia based on motion parameters of the simulator and the particular aircraft design being simulated. Finally, isocontours for both handling qualities and ride qualities are defined enabling future designers of transport aircraft to weigh the merits of their designs from both the passenger's and pilot's viewpoints. In addition, this can help a designer weigh the relative effects which some modification to an existing design would have on ride quality and passenger acceptance as well as handling quality and pilot acceptance. Also, the limitations of using ground-based simulators with restricted motion capabilities to measure ride quality are demonstrated.

For many years, a considerable amount of work, resources, and time have been spent by military and civil groups in the aeronautical

field to determine what qualities or characteristics an aircraft should have for it to be most easily and effectively flown. As a result, certain basic criteria have been formulated as guidelines for satisfactory aircraft handling qualities (1)-(8). In general, these criteria have been determined using variable stability aircraft. Stability parameters are varied within a limited range and the opinions of numerous pilots on the handling qualities of each configuration obtained. Handling qualities measurements are typically made in reasonably calm air, and results thus obtained are generally accepted to apply to high turbulence cases as well. This is not necessarily a prudent course to follow, in that turbulence can indeed have an effect on pilot opinion.

Gradually, the physical quantities which have a bearing on handling qualities were defined and the range of these parameters which delineate satisfactory and unsatisfactory handling qualities determined. Naturally, aircraft with different missions have vastly different requirements, thus handling qualities are different for a bomber or transport-type aircraft than for a high performance, highly maneuverable fighter.

However, even though much attention has been given in the past to developing aircraft with good handling qualities, very little attention has been devoted to developing aircraft with good ride qualities, i.e., aircraft in which the traveling public find flying pleasant (9). In the recent past, with the evolution of high-altitude jet aircraft, this has not presented serious problems since passengers on commercial flights, as a whole, were not especially annoyed by the

experience of flying. However, with the increasing use of short take-off and landing aircraft (STOL) in commercial operation, the question of acceptable levels of ride quality has arisen due to the often unpleasant nature of motion encountered on such aircraft (10).

STOL aircraft often exhibit objectionable ride qualities due to lower wing loadings or higher lift coefficients than aircraft used in conventional operations. Designs which use propulsive lift or thrust vectoring to attain STOL operations are generally not subject to ride-quality degradation because during the cruise portion of flight, these craft operate as high-wing loading conventional aircraft. It is not these designs at which this study is directed. Rather, it is the designs which achieve STOL performance by using low-wing loading. Wing loading is a measure of the lifting ability of a wing per unit of surface area. (For equilibrium flight, it is W/S, the aircraft weight divided by the wing reference area.) The lower the wing loading, the more susceptible the configuration is to external disturbances. Thus, low-wing loading aircraft are more severely disturbed by flight through rough air than high-wing loading designs, so it is to be expected that STOL aircraft would have worse ride qualities than conventional aircraft. It is just such aircraft with low-wing loadings which require modifications to improve their ride qualities.

During the past decade, considerable research has been conducted to determine what environmental and psychological factors define a person's state of comfort or discomfort. More specifically, human

response to motions of various forms, noise, temperature, and pressure levels have been measured and tolerance levels have been defined (11). A recent survey of past work done in this area is contained in Reference (12). With regard to the environment experienced by the flying public, the University of Virginia has been involved since 1970 in defining what factors are involved in determining passenger comfort, and have developed several comfort models based on aircraft motion parameters (13). This University of Virginia effort is based on simultaneous in-flight measurements of aircraft motions and sampling of passenger opinion on regional and commuter airlines on the East Coast.

To improve the ride quality of STOL aircraft, several means have been investigated (14). In general, these methods consist of placing sensors in the aircraft which sense aircraft motion, usually linear accelerations and angular rates. These signals are then used to deflect control surfaces which generate aerodynamic forces and moments which tend to minimize the motion which the passenger feels. One of the disadvantages of some of these systems is that they may tend to degrade the handling qualities or controllability of the airplane, making it more difficult or annoying for the pilot to fly. In addition to a weight penalty such systems may impose on a design, the failure of such a ride-control system may present a safety hazard by severely increasing pilot work load due to the corresponding change in handling qualities, or by exceeding design structural limits.

Rather than using active control systems to control ride quality, one might possibly design aircraft so that they are inherently pleasant

to ride. Thus, the purpose of this study is to determine the relationship between characteristic aircraft motions and aircraft ride quality.

Most aircraft have five distinct characteristic motions, two longitudinal and three lateral. These motions are determined by aircraft geometry, mass distribution, and flight conditions such as velocity and air density. The phugoid longitudinal mode and spiral lateral mode are normally of such long period that these pure motions would normally not be sensed by flying passengers. Periods and times to double/half amplitude of 30 seconds to two minutes are common for these modes. In fact, these modes are rarely seen in typical flight because these motions are readily damped out (usually unconsciously) by the pilot. Likewise, the rolling mode is not deemed important to aircraft ride quality because of the pilot's tendency to keep the wings level in cruise, and when maneuvering, to keep rolling rates small (usually less than 10 deg/sec). The two remaining aircraft modes, the Dutch Roll and the short-period modes, are of particular interest in ride-quality studies since their associated periods and amplitudes fall into the spectrum of motions found most uncomfortable by human beings (0 - 20 Hz) (12). The quantities which usually define the handling qualities of these two modes are the undamped natural frequency, ω_{n_s}, and the damping ratio, ζ_s, of the short-period mode, and the number of cycles to half amplitude, $C_{\frac{1}{2}_d}$, time to half amplitude, $T_{\frac{1}{2}_d}$, and a roll-to-sideslip parameter, $|\phi/v_e|_d$, for the Dutch Roll mode. Using the parameters established for defining satisfactory handling qualities for these two aircraft motions, the limits which satisfactory ride quality place on these parameters will be determined by subjecting

human subjects to such motion in aircraft simulators and eliciting their subjective comfort responses, and by using comfort models based on computed motion parameters for the simulator and the aircraft designs being studied.

The test program is divided into two distinct phases. The first phase investigated feasibility and the effects of varying certain parameters on ride and handling qualities. The range of parameter variation and the effects of these variations on ride quality were studied in the University of Virginia's Analog Flight Simulator.

Once these studies were completed, the second phase was initiated at NASA's Langley Research Center. Here tests were conducted on the Visual Motion Simulator (VMS) using aircraft parameters determined to be important in the first phase. Simultaneous measurements of both ride and handling qualities were made for various aircraft configurations and finally, the trade-offs between ride and handling qualities defined.

CHAPTER II

SIMULATOR EXPERIMENTS AT THE UNIVERSITY OF VIRGINIA

The University of Virginia's fixed-base analog flight simulator (Figure 1 and Appendix A) was programmed with the six-degree-of-freedom equations of motion (Appendix B) given in Figure 2. The aircraft used in the simulation was a 51152 N (11,500 pound) Canadian deHavilland DHC-6 Twin Otter. This particular aircraft was chosen because it is a typical STOL aircraft and has been in service since 1966 in many roles. Also, its flying characteristics are well known, and there are many pilots available with flying experience in the Twin Otter to validate the ground-based simulations. Flight conditions of level flight at 914.4 m (3000 feet) and an equilibrium flight speed of 78.2 m/s (175 mph) were chosen as the typical environment in which this aircraft is operated in present short-haul commuter service on the East Coast. The wing loading of the aircraft in this configuration is 405.2 N/m^2 (27.4 lb/ft^2). Based on these flight conditions, stability derivatives were obtained from an unpublished NASA document containing a mathematical model for the Twin Otter used in a fixed-base simulation at the Langley Research Center to study STOL air traffic control procedures. These stability derivatives agree well with ones contained in Reference (14) for a Twin Otter in approximately the same flight conditions. The stability derivatives for this flight condition may be found in Table I using standard NACA notation (see Appendices C and D). This condition and its corresponding set of stability derivatives will be referred to as the "nominal" conditions.

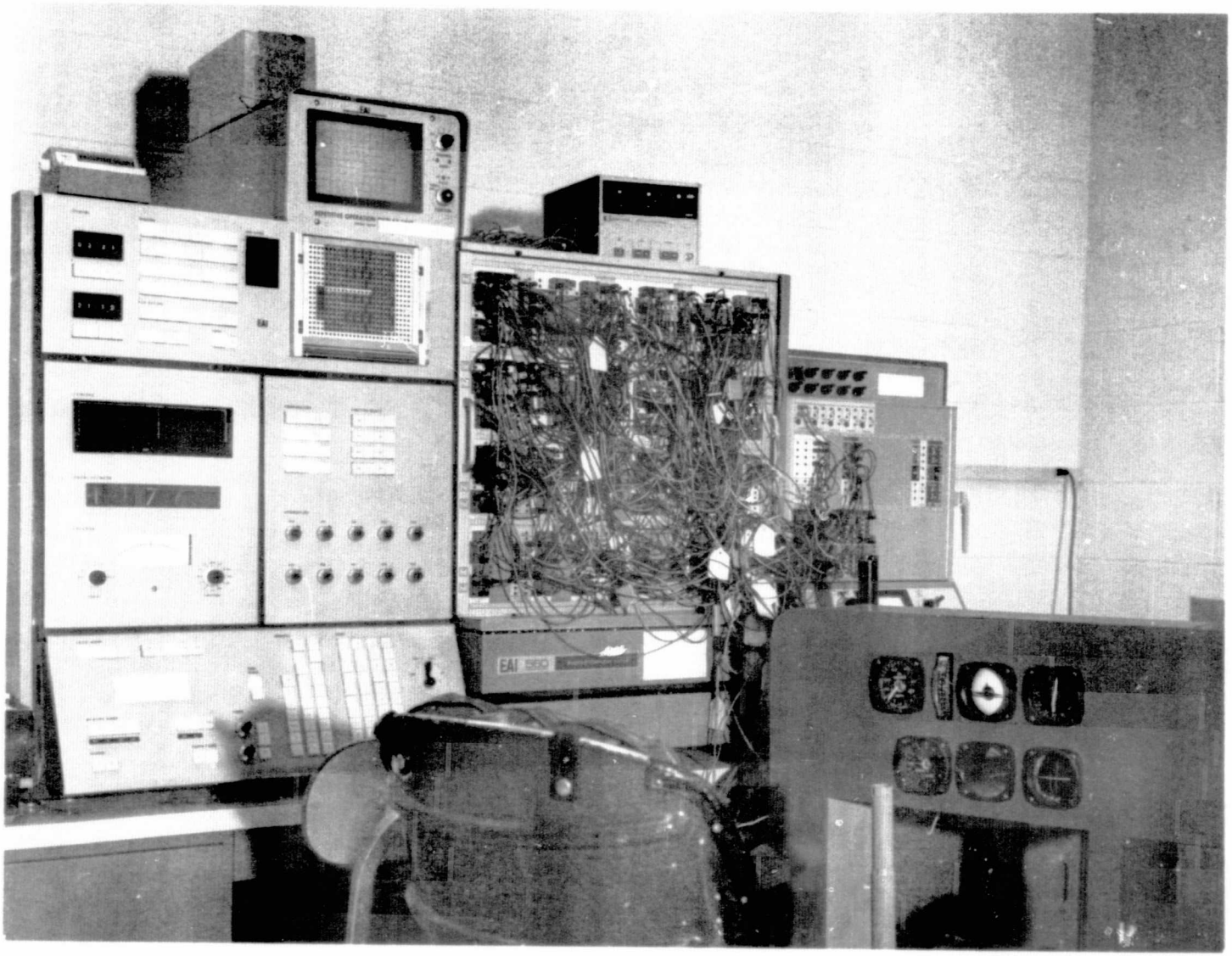

FIGURE 1. THE UNIVERSITY OF VIRGINIA'S ANALOG FLIGHT SIMULATOR

$$-\dot{u} = -\dot{\psi}\beta + \dot{\theta}\alpha + \left[-\frac{C_{x_u} Sq_\infty}{mU_0}\right] u - \left[\frac{Sq_\infty \bar{c}}{2mU_0^2} C_{x_{\dot{\alpha}}}\right] \dot{\alpha} + \left[\frac{C_{x_\alpha} Sq_\infty}{mU_0}\right] \alpha$$

$$+ \left[\frac{Sq_\infty \bar{c}}{2mU_0^2} C_{x_q}\right] \dot{\theta} + \left[\frac{g}{U_0}\right] \theta - \left[\frac{Sq_\infty C_{x_{\delta_T}}}{mU_0}\right] \delta_T$$

$$-\dot{\alpha} = -\left[\frac{\frac{mU_0}{Sq_\infty} + \frac{\bar{c}}{2U_0} C_{z_q}}{\frac{mU_0}{Sq_\infty} - \frac{\bar{c}}{2U_0} C_{z_{\dot{\alpha}}}}\right] \dot{\theta} - \left[\frac{\frac{mU_0}{Sq_\infty}}{\frac{mU_0}{Sq_\infty} - \frac{\bar{c}}{2U_0} C_{z_{\dot{\alpha}}}}\right] \dot{\theta} u + \left[\frac{\frac{mU_0}{Sq_\infty}}{\frac{mU_0}{Sq_\infty} - \frac{\bar{c}}{2U_0} C_{z_{\dot{\alpha}}}}\right] \dot{\phi}\beta$$

$$+ \left[\frac{C_{z_u}}{-\frac{mU_0}{Sq_\infty} + \frac{\bar{c}}{2U_0} C_{z_{\dot{\alpha}}}}\right] u + \left[\frac{C_{z_\alpha}}{-\frac{mU_0}{Sq_\infty} + \frac{\bar{c}}{2U_0} C_{z_{\dot{\alpha}}}}\right] \alpha - \left[\frac{\bar{c}}{\ell_t}\right]\left[\frac{C_{m_{\delta_e}}}{\frac{mU_0}{Sq_\infty} - \frac{\bar{c}}{2U_0} C_{z_{\dot{\alpha}}}}\right] \delta_e$$

$$-\ddot{\theta} = -\left[\frac{Sq_\infty \bar{c} C_{m_u}}{I_y}\right] u + \left[-\frac{Sq_\infty \bar{c}^2 C_{m_{\dot{\alpha}}}}{2U_0 I_y}\right] \dot{\alpha} + \left[-\frac{Sq_\infty \bar{c}}{I_y} C_{m_\alpha}\right] \alpha$$

$$+ \left[-\frac{Sq_\infty \bar{c}^2}{2U_0 I_y} C_{m_q}\right] \dot{\theta} - \left[\frac{C_{m_{\delta_e}} Sq_\infty \bar{c}}{I_y}\right] \delta_e$$

$$-\dot{\beta} = -\dot{\phi}\alpha + \dot{\psi} + \dot{\psi} u - \left[\frac{Sq_\infty}{mU_0} C_{y_\phi}\right] \phi - \left[\frac{Sq_\infty b}{2mU_0^2} C_{y_r}\right] \dot{\psi} + \left[-\frac{Sq_\infty C_{y_\beta}}{mU_0}\right] \beta$$

$$- \left[\frac{Sq_\infty}{mU_0} C_{y_{\delta_r}}\right] \delta_r - \left[\frac{Sq_\infty b}{2mU_0^2} C_{y_p}\right] \dot{\phi}$$

$$-\ddot{\phi} = + \left[-\frac{Sq_\infty b^2}{2U_0 I_x} C_{\ell_p}\right] \dot{\phi} - \left[\frac{Sq_\infty b^2}{2U_0 I_x} C_{\ell_r}\right] \dot{\psi} + \left[-\frac{Sq_\infty b}{I_x} C_{\ell_\beta}\right] \beta$$

$$- \left[\frac{Sq_\infty b}{I_x} C_{\ell_{\delta_a}}\right] \delta_a - \left[\frac{Sq_\infty b}{I_x} C_{\ell_{\delta_r}}\right] \delta_r$$

$$-\ddot{\psi} = + \left[-\frac{Sq_\infty b^2}{2U_0 I_z} C_{n_p}\right] \ddot{\phi} + \left[-\frac{Sq_\infty b^2}{2U_0 I_z} C_{n_r}\right] \dot{\psi} - \left[\frac{Sq_\infty b}{I_z} C_{n_\beta}\right] \beta$$

$$+ \left[-\frac{Sq_\infty b}{I_z} C_{n_{\delta_a}}\right] \delta_a + \left[-\frac{Sq_\infty b}{I_z} C_{n_{\delta_r}}\right] \delta_r$$

FIGURE 2. EQUATIONS OF MOTION

TABLE I

FLIGHT CONDITIONS (EQUILIBRIUM)

h = 914.4 m (3000 ft) (level flight)

W = 51152 N (11500 lb)

U_0 = 78.2 m/s (256.67 ft/sec, 175 mph)

ρ = 1.122 kg/m^3 (0.002177 slug/ft^3)

C_T = 0.045

h^* = 0.2

I_x = 22907 kg-m^2 (16900 slug-ft^2)

I_y = 37411 kg-m^2 (27600 slug-ft^2)

I_z = 55031 kg-m^2 (40600 slug-ft^2)

I_{xz} = 1898 kg-m^2 (1400 slug-ft^2)

α_0 = -1.3°

$\bar{c}$ = 1.98 m (6.5 ft)

b = 19.8 m (65 ft)

S = 39.0 m^2 (420 ft^2)

δ_{flap} = 0

TURBULENCE CONDITIONS

$\sigma_v = \sigma_w$ = 0.914 m/s (3 fps)

σ_u = 0

NOMINAL STABILITY DERIVATIVES

Longitudinal Derivatives

C_L = 0.3818

C_D = 0.045

C_M = 0.035

C_{L_α} = 5.7295

C_{D_α} = 0.1432

C_{m_α} = -1.9098

$C_{L_{\dot\alpha}}$ = 1.52

$C_{D_{\dot\alpha}}$ = 0

$C_{m_{\dot\alpha}}$ = -5.9

C_{L_q} = 5.504

C_{D_q} = 0

C_{m_q} = -23.948

C_{x_u} = -2 C_D

C_{z_u} = -2 C_L

C_{x_α} = C_L - C_{D_α}

C_{z_α} = -C_{L_α} - C_D

$C_{x_{\dot\alpha}}$ = -$C_{D_{\dot\alpha}}$

$C_{z_{\dot\alpha}}$ = -$C_{L_{\dot\alpha}}$

C_{x_q} = -C_{D_q}

C_{z_q} = -C_{L_q}

TABLE I (Continued)

Lateral Derivatives

$C_{y_\beta} = -0.89$
$C_{\ell_\beta} = -0.12$
$C_{n_\beta} = 0.1215$

$C_{y_p} = -0.1$
$C_{\ell_p} = -0.5488$
$C_{n_p} = 0.006$

$C_{y_r} = 0.5$
$C_{\ell_r} = 0.13$
$C_{n_r} = -0.1855$

Control Derivatives

$C_{y_{\delta_r}} = 0.39$
$C_{y_{\delta_a}} = 0.00348$
$C_{\ell_{\delta_a}} = 0.2055$
$C_{\ell_{\delta_r}} = 0.0398$

$C_{n_{\delta_r}} = -0.1$
$C_{n_{\delta_a}} = -0.01$
$C_{m_{\delta_e}} = -1.79$
$C_{L_{\delta_e}} = 0.45$

In addition to the nominal configuration, other stability conditions were run. These conditions were produced by varying C_{m_α} ($= \partial C_m/\partial\alpha$, the slope of the pitching moment curve) and C_{m_q} ($= \partial C_m/\partial q \doteq \partial C_m/\partial\dot{\theta}$, the pitch damping derivative) in the longitudinal mode, and C_{y_β} ($= \partial C_y/\partial\beta$, the side-force damping derivative) and C_{n_β} ($= \partial C_n/\partial\beta$, the static directional derivative or weathercock stability derivative) in the lateral mode. The longitudinal parameters were varied holding the lateral derivatives at the nominal conditions and the lateral derivatives were varied holding the longitudinal derivatives at their nominal values.

As an approximation of the short-period mode (15), it can be shown that the natural frequency, ω_{n_s}, is given by

$$\omega_{n_s}^2 \approx (C_{z_\alpha} C_{m_q}) \frac{\bar{c}}{2U_0} - (C_{m_\alpha}) \frac{mU_0}{q_\infty S}$$

and the damping ratio, ζ_s, by

$$2\zeta_s \omega_{n_s} \approx \frac{\bar{c}m}{2Sq_\infty} (-C_{m_q} - C_{m_{\dot{\alpha}}}) - \frac{I_y}{Sq_\infty \bar{c}} C_{z_\alpha} ,$$

where

$\bar{c}$ = longitudinal reference length, mean aerodynamic chord

I_y = moment of inertia about the pitch axis

m = aircraft mass

q_∞ = dynamic pressure, $\frac{1}{2}\rho U_0^2$

U_0 = equilibrium flight speed.

Thus, by judicious choice of C_{m_α} and C_{m_q} a designer could obtain any set of ω_{n_s} and ζ_s for the short-period mode he would desire, holding all other parameters constant. The primary factor which determines C_{m_α} is the static margin, the distance which the aircraft center of gravity is in front of the center of pressure. For example, the designer, by proper selection of center of gravity location, may select a desired value of C_{m_α}. The value of the stability derivative C_{m_q} is determined by the size and location of the horizontal tail. Therefore, by choosing a horizontal tail of appropriate size and locating it a specified distance behind the center of gravity, the designer can obtain a desired value of C_{m_q}. Hence the designer has control over the defining parameters for the short-period mode, but he must be aware of how his variations of C.G. location and tail size and location might affect other stability derivatives (e.g., $C_{m_{\dot{\alpha}}}$) and what ramifications such variations would have on cost, complexity, and mission performance of a particular configuration.

Likewise, C_{y_β} and C_{n_β} are dominant factors which determine the damping and frequency of the Dutch Roll mode and are therefore important to the handling qualities of the Dutch Roll mode. For simplicity in this study, only variations in C_{y_β} and C_{n_β} were used to modify Dutch Roll characteristics. However, other stability derivatives, such as C_{ℓ_β} and C_{n_r}, have direct effects of Dutch Roll characteristics and, at the designers option, he may wish to vary these in addition to, or instead of C_{y_β} and C_{n_β}. The values of C_{y_β} and C_{n_β} are largely determined by the size and location of the vertical tail; thus the designer, by giving appropriate attention to

the matter, may choose a design which will give him values for C_{y_β}, C_{n_β}, C_{n_r}, and C_{ℓ_β} which will result in good handling qualities in the Dutch Roll mode.

For each set of stability derivatives to be investigated, the fourth-degree longitudinal and lateral equations of motion were solved for their characteristic roots. From these characteristic values, the short-period undamped natural frequency, ω_{n_s} and the damping ratio, ζ_s were computed from the longitudinal roots. Also, the number of cycles to half amplitude, $C_{\frac{1}{2}_d}$, the time to half amplitude, $T_{\frac{1}{2}_d}$, and the roll-to-sideslip parameter, $|\phi/v_e|_d$ for the Dutch Roll mode were found from the lateral roots. $C_{\frac{1}{2}_d}$ and $T_{\frac{1}{2}_d}$ are related to the undamped natural frequency, ω_{n_d}, and damping ratio, ζ_d, of the Dutch Roll mode by the following expressions:

$$C_{\frac{1}{2}_d} = \frac{-\ln(\frac{1}{2})}{2\pi} \frac{\sqrt{1-\zeta_d^2}}{\zeta_d}$$

$$T_{\frac{1}{2}_d} = \frac{\ln(\frac{1}{2})}{-\zeta_d \omega_{n_d}} .$$

$|\phi/v_e|_d$ is related in a complex way to ω_{n_d} and ζ_d and is found by the relation

$$|\phi/v_e|_d = \frac{1}{U_0} |\phi/\beta|_d$$

where $|\phi/\beta|_d$ is found by a modal analysis of the lateral equations solved at the Dutch Roll ω_{n_d} and ζ_d.

It is these quantities which are used to define a design's short-period and Dutch Roll handling qualities (1)-(8). For the longitudinal short-period mode, the natural frequency and damping ratio describe the response of an aircraft to an abrupt pitch change from equilibrium flight and its subsequent return to equilibrium conditions. Similarly, for the lateral Dutch Roll mode, $C_{\frac{1}{2}_d}$ and $T_{\frac{1}{2}_d}$ describe the motion of an aircraft after being disturbed from equilibrium heading, roll, and sideslip conditions. The roll-to-sideslip parameter is a measure of the roll induced for a unit lateral gust and is a gauge of an aircraft's lateral responsiveness.

The analog flight simulator was programmed with various combinations of stability derivatives to cover, as well as possible, the regions in which handling qualities are most often defined for the short-period and Dutch Roll aircraft modes. Coupled to the analog computer was an electronic noise generator adjusted to disturb the simulated aircraft with .914 m/s (3 ft/sec) rms turbulent gusts in the normal and lateral directions. This was accomplished by superimposing the random electronic signal on the α and β variables in the analog equations of motion. The simulated turbulence was essentially random noise with the spectrum shown in Figure 3.

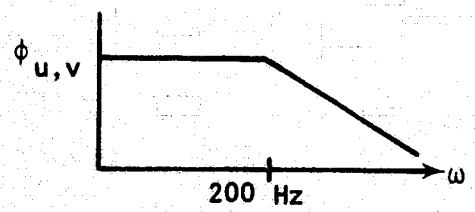

FIGURE 3. GUST INPUT POWER SPECTRUM

For each different aircraft configuration, the simulator was operated at least 12 times while a pilot flew the simulator attempting to maintain straight and level flight for over 200 seconds. This run duration was chosen to permit the rms normal and transverse accelerations computed by the analog computer to stabilize at a steady-state value. The associated comfort rating for each flight was found by using an empirically-derived comfort model developed at the University of Virginia (16) using their comfort-rating scale. (See Table II.) This particular model was chosen for its relative simplicity and because its defining parameters could be obtained from the analog computer with relative ease. The model was derived by simultaneously recording aircraft motion and sampling passenger opinion of ride quality on regional and commuter airlines during actual flight operations on the East Coast. This data was then statistically analyzed and a best fit curve determined (13). Finally, the average rating for each aircraft configuration was found and converted into a passenger satisfaction level by a statistically-determined transformation (17), shown in Figure 4. This relationship was formulated by analysis of questionnaire data recorded on the above-mentioned commercial flights asking the passengers to report their comfort levels and their willingness to take another flight based on their recent flight environment.

The values of passenger satisfaction due to variations in the short-period handling qualities are plotted in Figure 5. The solid lines in this figure indicate the presently accepted boundaries for short-period handling qualities. The dashed lines indicate lines of constant ride quality, as suggested by the data points. The trend is

TABLE II

COMFORT RATING SCALE

1 - Very comfortable

2 - Comfortable

3 - Neutral

4 - Uncomfortable

5 - Very uncomfortable

COMFORT MODEL

$$CR = 2 + 13.8\, a_N + 4.52\, a_T - 2.816 \sqrt{a_N a_T}$$

where a_N = normal rms acceleration (g's)

a_T = transverse rms acceleration (g's)

CR = comfort rating (1-5)

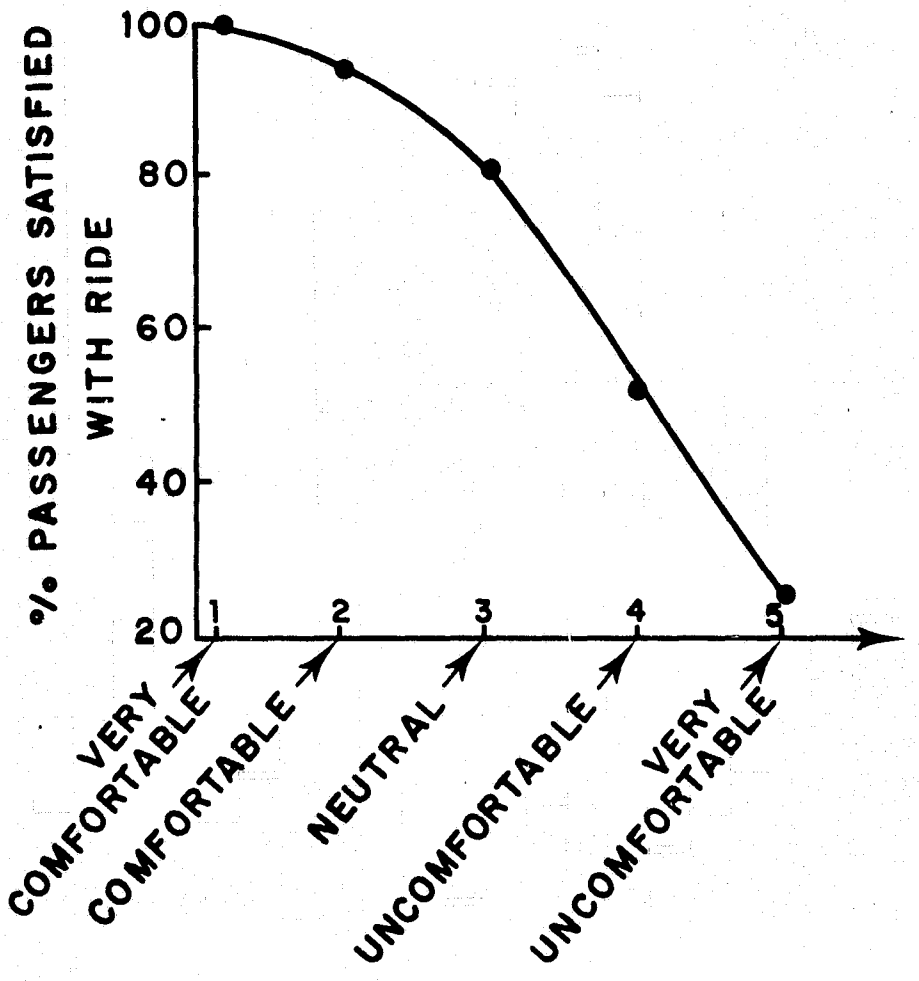

MATHEMATICAL FIT TO THE CURVE

$$\% = \frac{-B - \sqrt{B^2 - 4C(A - CR)}}{2C} \qquad CR < 3$$

$A = -159/11$

$B = 26/55$

$C = -0.035/11$

$$\% = 162.5 - 27.5\,CR \qquad CR \geq 3$$

FIGURE 4. RELATIONSHIP BETWEEN PASSENGER SATISFACTION AND COMFORT RATING

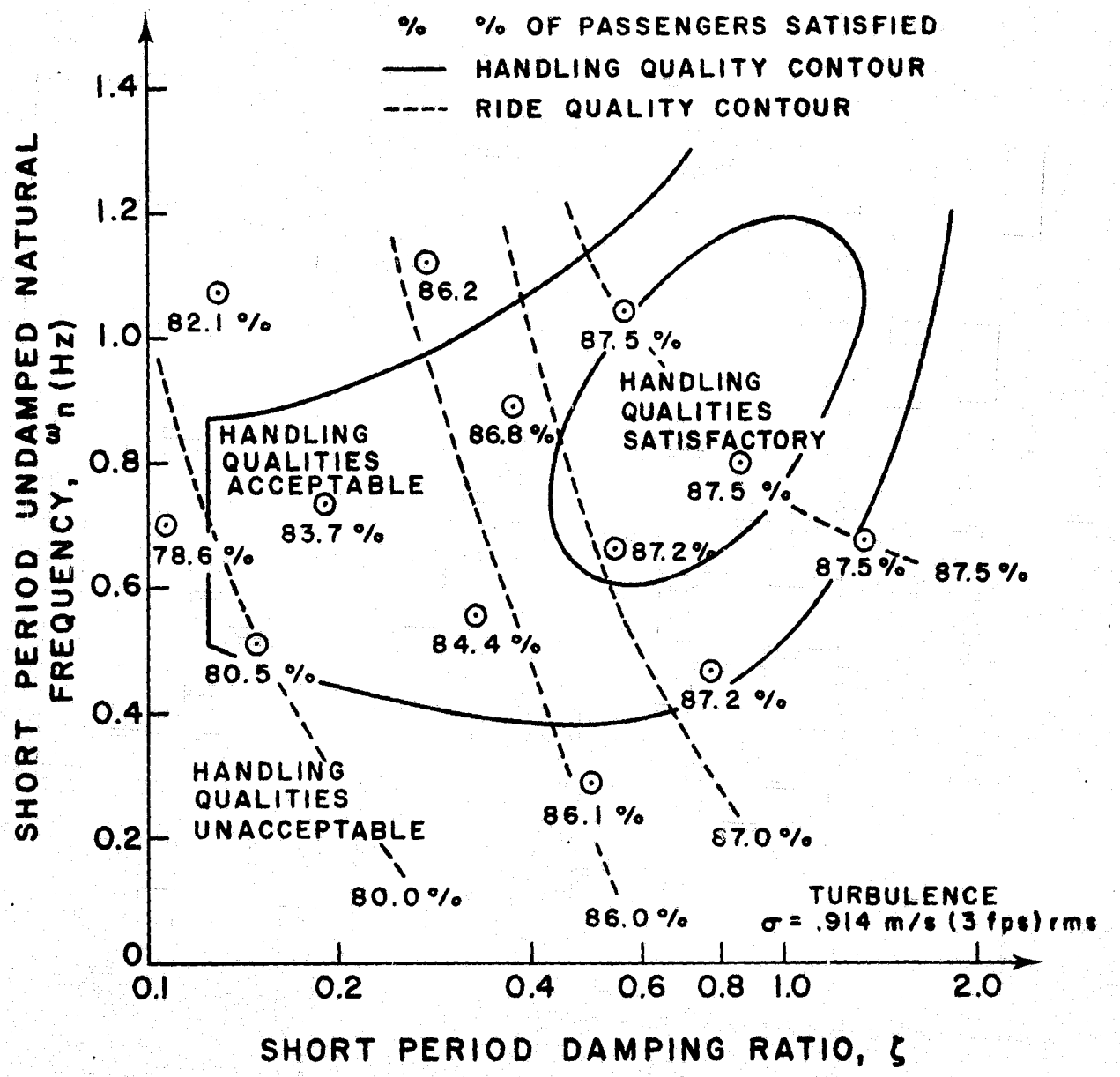

FIGURE 5. SHORT-PERIOD HANDLING QUALITIES

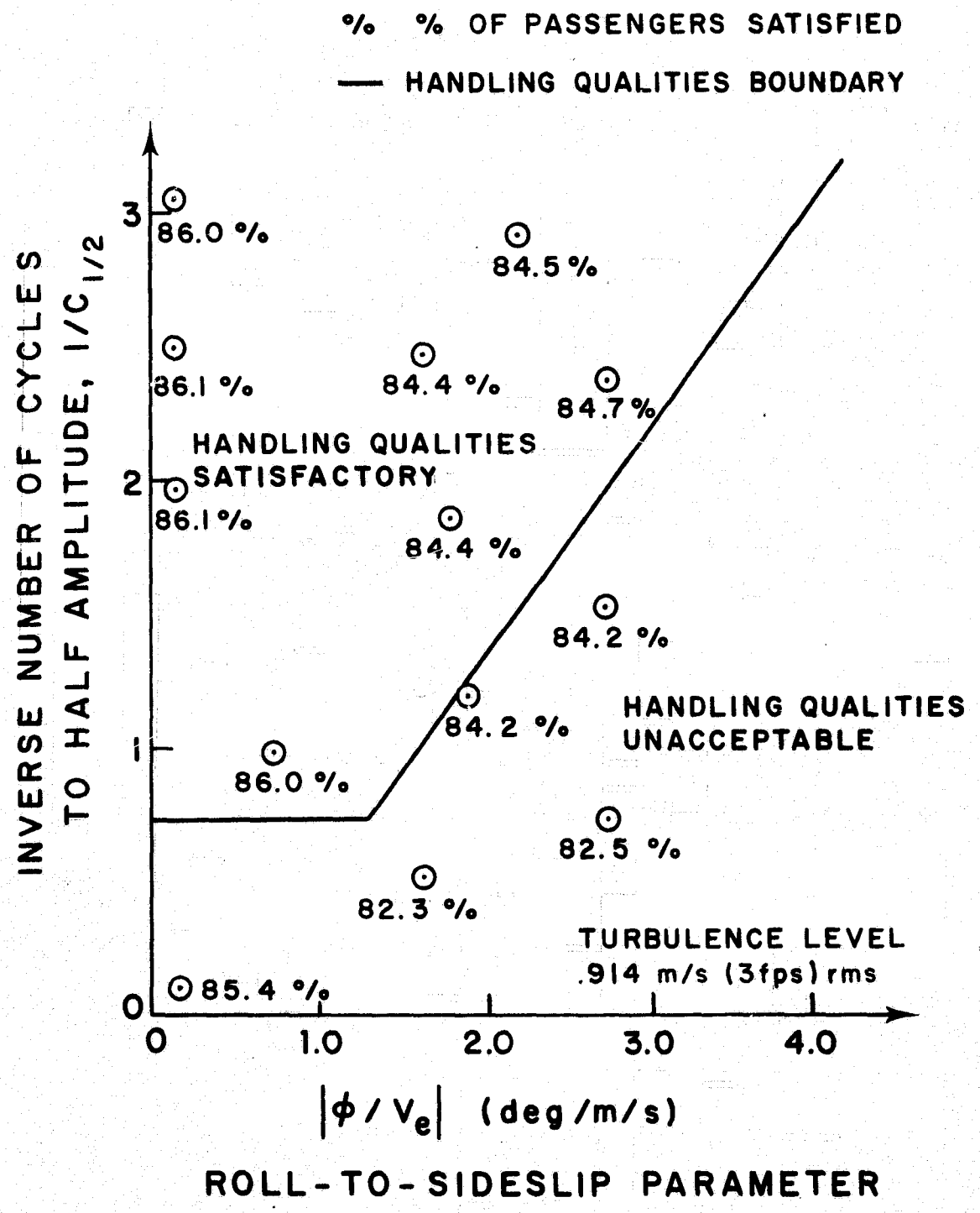

FIGURE 6. DUTCH ROLL HANDLING QUALITIES
($1/C_{\frac{1}{2}}$ vs. $|\phi/v_e|$)

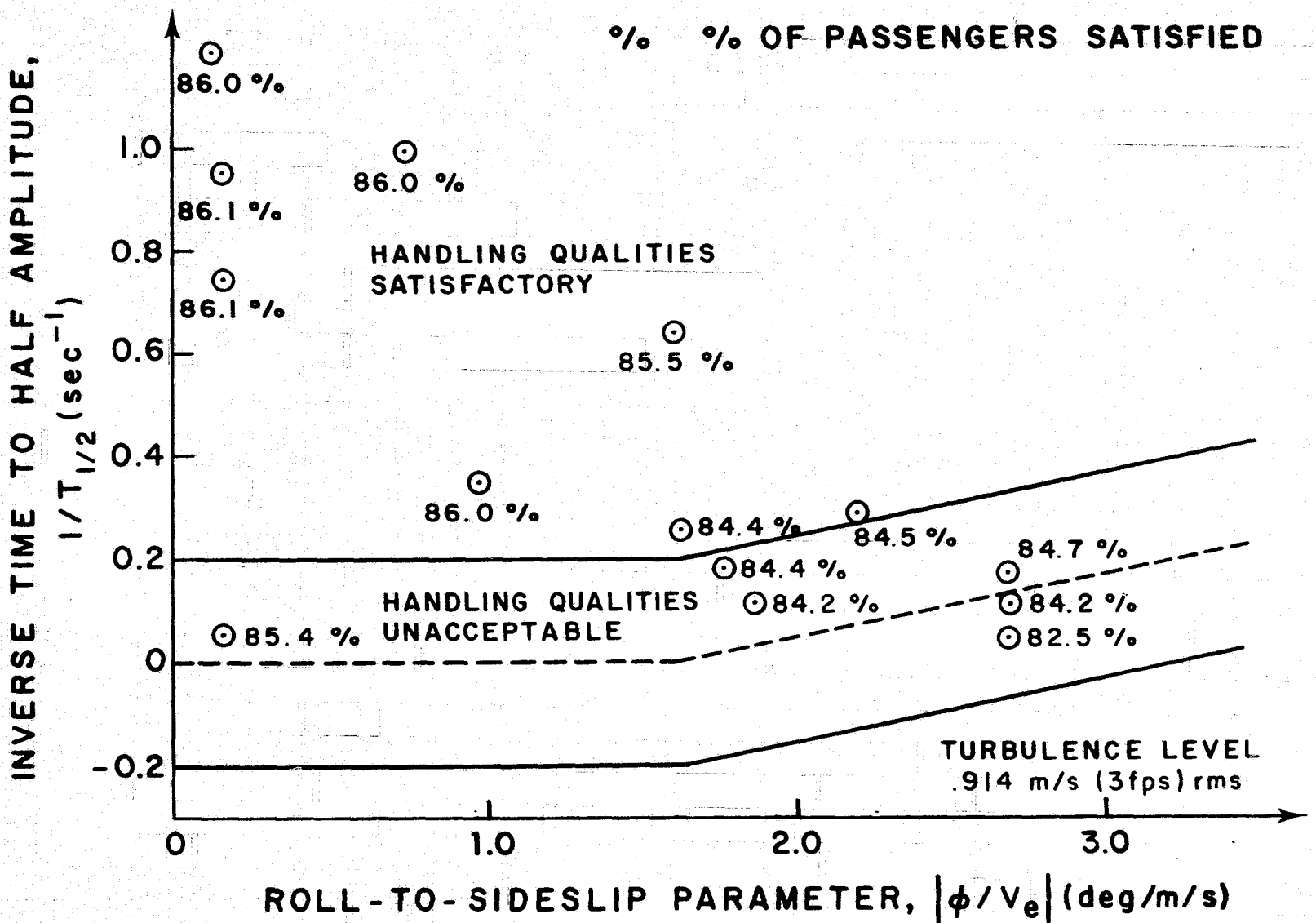

FIGURE 7. DUTCH ROLL HANDLING QUALITIES
($1/T_{\frac{1}{2}}$ vs. $|\phi/v_e|$)

for increasing passenger satisfaction as the damping ratio and the undamped natural frequency increase. These trends are to be expected, since an increase in damping ratio will directly result in decreasing normal acceleration and improving ride quality. Further, increasing the natural frequency tends to make a design more responsive, allowing a pilot to better maintain control and keep motion to a minimum, also improving ride quality.

The effects of variations of Dutch Roll parameters on ride quality are shown in Figures 6 and 7. The solid line indicates boundaries for regions of acceptable Dutch Roll handling. Ride quality and passenger acceptance generally improve as $C_{\frac{1}{2}_d}$, $T_{\frac{1}{2}_d}$, and $|\phi/v_e|_d$ decrease, although the trends are not as clear as those of the short-period mode. Again, this might be expected since decreasing the number of cycles to half amplitude and the time to half amplitude corresponds to increasing the damping of the Dutch Roll mode and reducing lateral acceleration. Likewise, decreasing the roll-to-sideslip parameter implies reduction of the aircraft roll response to lateral gusts resulting in lower lateral accelerations and better ride qualities. Also, it appears that the changes in longitudinal short-period parameters had a greater effect on ride quality than did the changes in the Dutch Roll parameters.

No attempt was made in this part of the study to measure pilot opinion since a pilot experienced in evaluating handling qualities was not available and no motion or visual cues are provided by the simulator.

CHAPTER III

SIMULATOR EXPERIMENTS AT THE NASA LANGLEY RESEARCH CENTER

Using the data and experience gained during the tests on the University of Virginia's Analog Flight Simulator, 27 different sets of stability derivatives were selected to be studied further at the NASA Langley Research Center. Fourteen longitudinal cases and 12 lateral cases were chosen in addition to the "nominal" set of Twin Otter stability derivatives contained in Table I of the previous section. These cases and the corresponding flight conditions are contained in Table III. These cases were chosen to cover the regions in which longitudinal and lateral handling qualities are most often defined for the short-period and Dutch Roll modes by aircraft designers. Figure 8 shows the contours which define longitudinal short-period handling qualities as a function of undamped natural frequency, ω_{n_s}, and damping ratio, ζ_s. The numbered points on this figure indicate the 14 test cases studied, plus the nominal case. Similarly, Figures 9 and 10 depict the 12 lateral test cases studied, plus the nominal case plotted in terms in which the Dutch Roll handling qualities are normally defined, namely the number of cycles to half amplitude, the time to half amplitude, and the roll-to-sideslip parameter.

The Visual Motion Simulator (VMS) at the NASA Langley Research Center, a synergistic motion-based simulator with the basic interior and instrumentation of a jet transport cockpit (Figures 11 and 12), was programmed with the 27 test cases described. A schematic diagram of

TABLE III

FLIGHT CONDITIONS (EQUILIBRIUM)

h = 914.4 m (3000 ft) (level flight)

W = 51152 N (11500 lb)

U_0 = 78.2 m/s (175 mph = 256.67 ft/sec)

ρ = 1.122 kg/m^3

C_T = 0.045

h^* = 0.2

I_x = 22907 kg-m^2 (16900 slug-ft^2)

I_y = 37411 kg-m^2 (27600 slug-ft^2)

I_z = 55031 kg-m^2 (40600 slug-ft^2)

I_{xz} = 1898 kg-m^2 (1400 slug-ft^2)

α_0 = -1.3°

$\bar{c}$ = 1.98 m (6.5 ft)

b = 19.8 m (65 ft)

S = 39.0 m^2 (420 ft^2)

δ_{flap} = 0

TURBULENCE CONDITIONS

(DRYDEN MODEL)

Spectra

$$\phi_u(\omega) = \sigma_u^2 \frac{2L_u}{\pi U_0} \frac{1}{1 + (L_u\omega/U_0)^2}$$

$$\phi_v(\omega) = \sigma_v^2 \frac{L_v}{\pi U_0} \left(\frac{1 + 3(L_v\omega/U_0)^2}{[1 + (L_v\omega/U_0)^2]^2} \right)$$

$$\phi_w(\omega) = \sigma_w^2 \frac{L_w}{\pi U_0} \left(\frac{1 + 3(L_w\omega/U_0)^2}{[1 + (L_w\omega/U_0)^2]^2} \right)$$

$\sigma_u = \sigma_v = \sigma_w$ = 1.524 m/s (5 ft/sec)

$L_u = L_v = L_w$ = 762 m (2500 ft)

Pilot Position with Respect to Aircraft c.g.

x = 2.7 m (8.8 ft) y = -.49 m (-1.6 ft) z = 0

TABLE III (Continued)

LONGITUDINAL TEST CASES

			Short-period Mode	
Case Number	C_{m_α}	C_{m_q}	ω_{n_s} (cps)	ζ_s
2	-1.9098	0	0.577	0.332
3	-4.0	-20.0	0.885	0.377
4	-0.64	-23.948	0.463	0.782
5	-6.76	-23.948	1.132	0.320
6	-3.24	7.0	0.731	0.193
7	-0.64	7.0	0.286	0.499
8	-1.9098	-70.0	0.796	0.868
9	-4.84	-56.0	1.041	0.568
10	-0.16	-101.0	0.677	1.347
11	-2.56	-119.0	0.978	1.065
12	-5.76	-119.0	1.231	0.846
13	-1.9098	16.0	0.514	0.150
19	-3.24	16.0	0.704	0.109
20	-6.76	7.0	1.072	0.132

TABLE III (Continued)

LATERAL TEST CASES

Case Number	C_{n_β}	C_{y_β}	$1/C_{\frac{1}{2}_d}$	Dutch Roll Mode $1/T_{\frac{1}{2}_d}$ (sec^{-1})	Dutch Roll Mode $\lvert\phi/v_e\rvert_d$ ($^o/m/s$)
14	0.01583	0.62	2.485	0.260	1.699
15	0.81	-0.89	0.999	0.984	0.766
16	0.1215	-1.875	3.076	1.184	0.160
17	0	-1.0	2.384	0.171	2.736
18	0.01417	0.86	1.193	0.115	1.914
21	0.1215	0	1.978	0.743	0.165
22	0.01167	0.82	0.504	0.045	2.098
23	0.015	0.74	1.864	0.186	1.810
24	0	-0.75	1.533	0.112	2.737
25	0.25	3.0	0.107	0.055	0.194
26	0	-0.5	0.721	0.053	2.738
27	0.0075	-0.25	2.939	0.243	2.231

TABLE III (Continued)

NOMINAL CONDITIONS

Case Number 1

$C_{m_\alpha} = -1.9098$

$C_{m_q} = -23.948$

$C_{n_\beta} = 0.1215$

$C_{y_\beta} = -0.89$

Short-period Mode

$\omega_{n_s} = 0.660$ cps

$\zeta_s = 0.549$

Dutch Roll Mode

$1/C_{t_{\frac{1}{2}_d}} = 2.501$

$1/T_{t_{\frac{1}{2}_d}} = 0.953/\text{sec}$

$|\phi/v_e|_d = 0.1627\ ^\circ/\text{m/sec}$

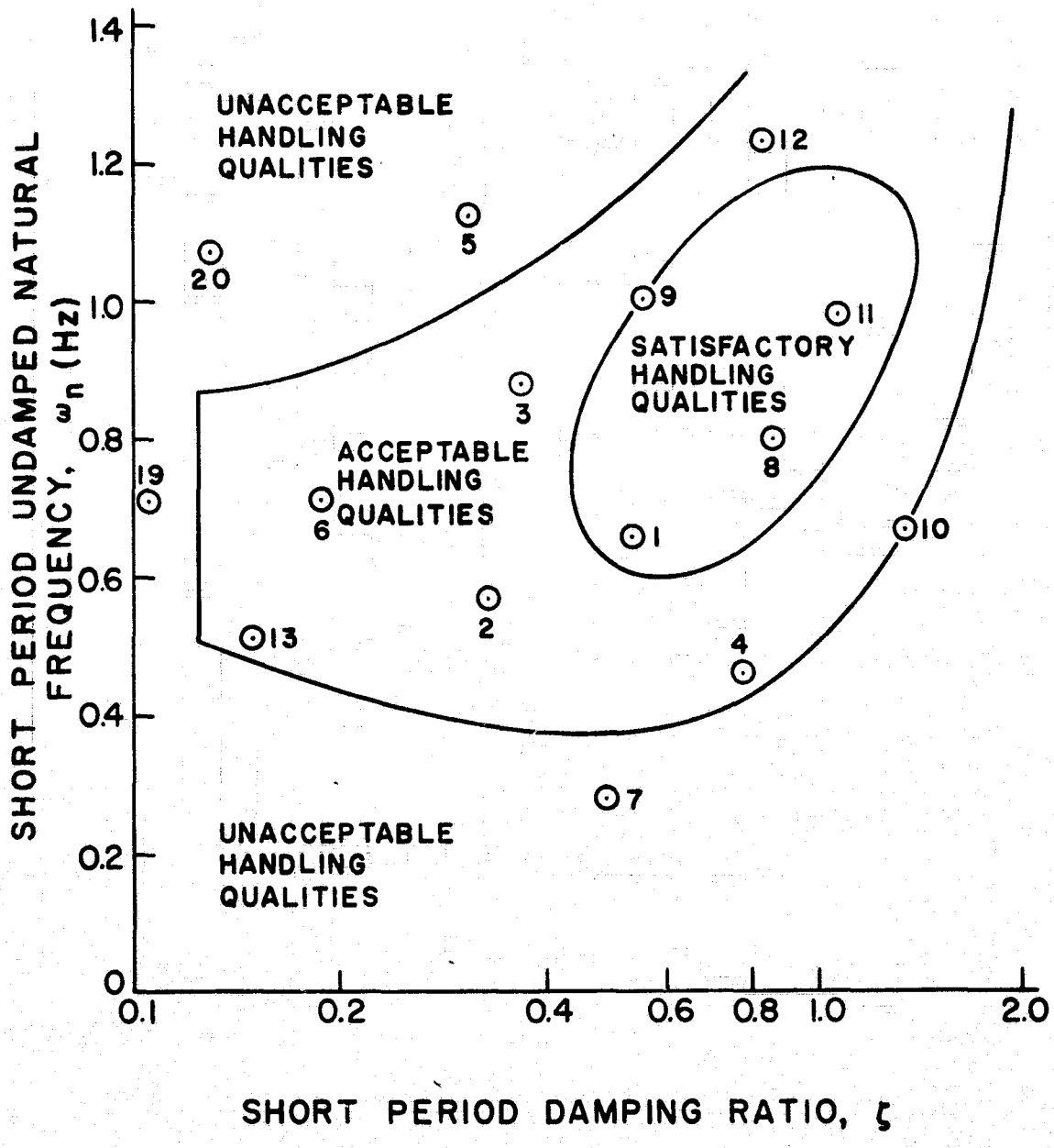

FIGURE 8. SHORT-PERIOD HANDLING QUALITIES BOUNDARIES AND LONGITUDINAL TEST CASES

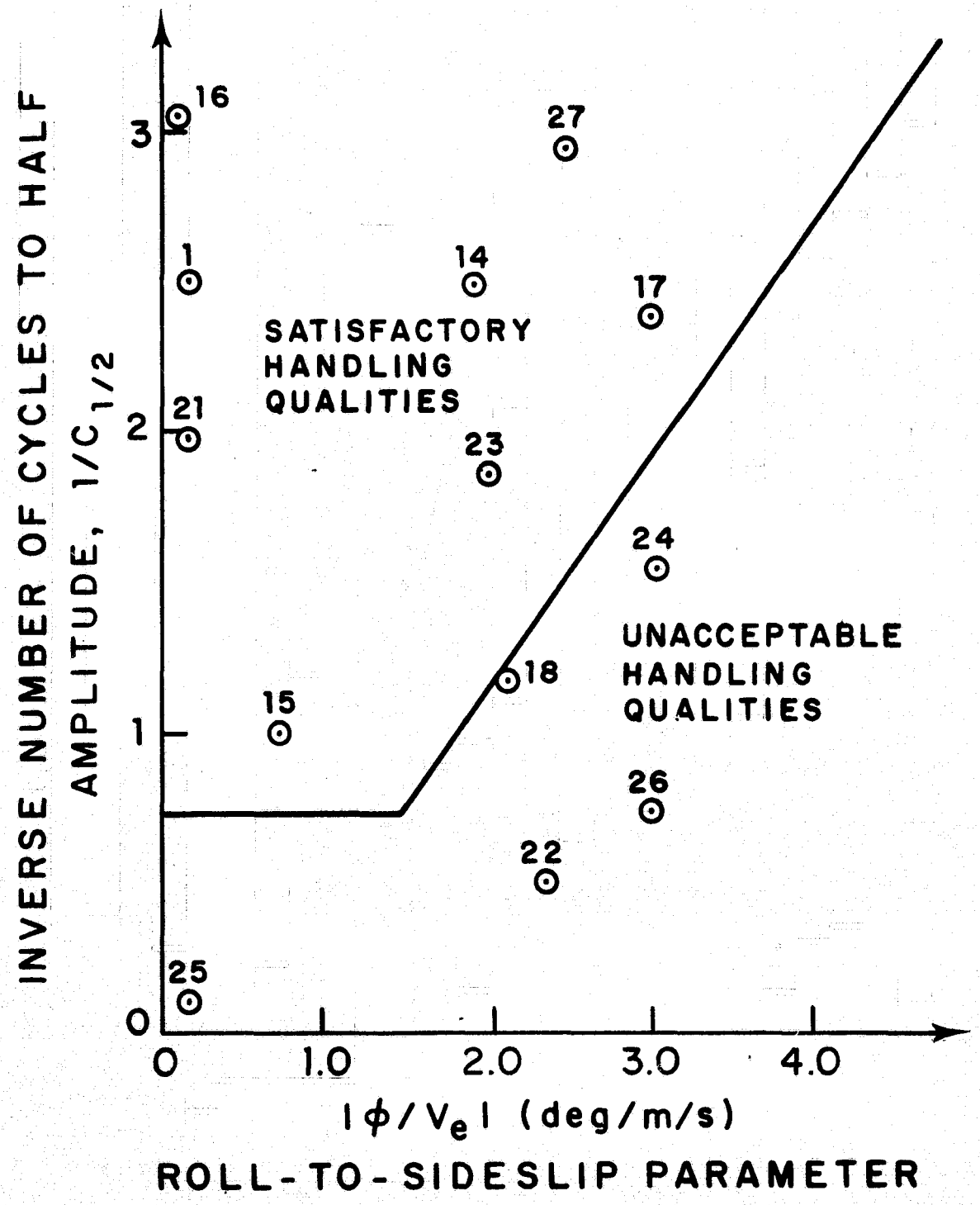

FIGURE 9. DUTCH ROLL HANDLING QUALITIES BOUNDARIES AND LATERAL TEST CASES, ($1/C_{\frac{1}{2}}$ vs. $|\phi/v_e|$)

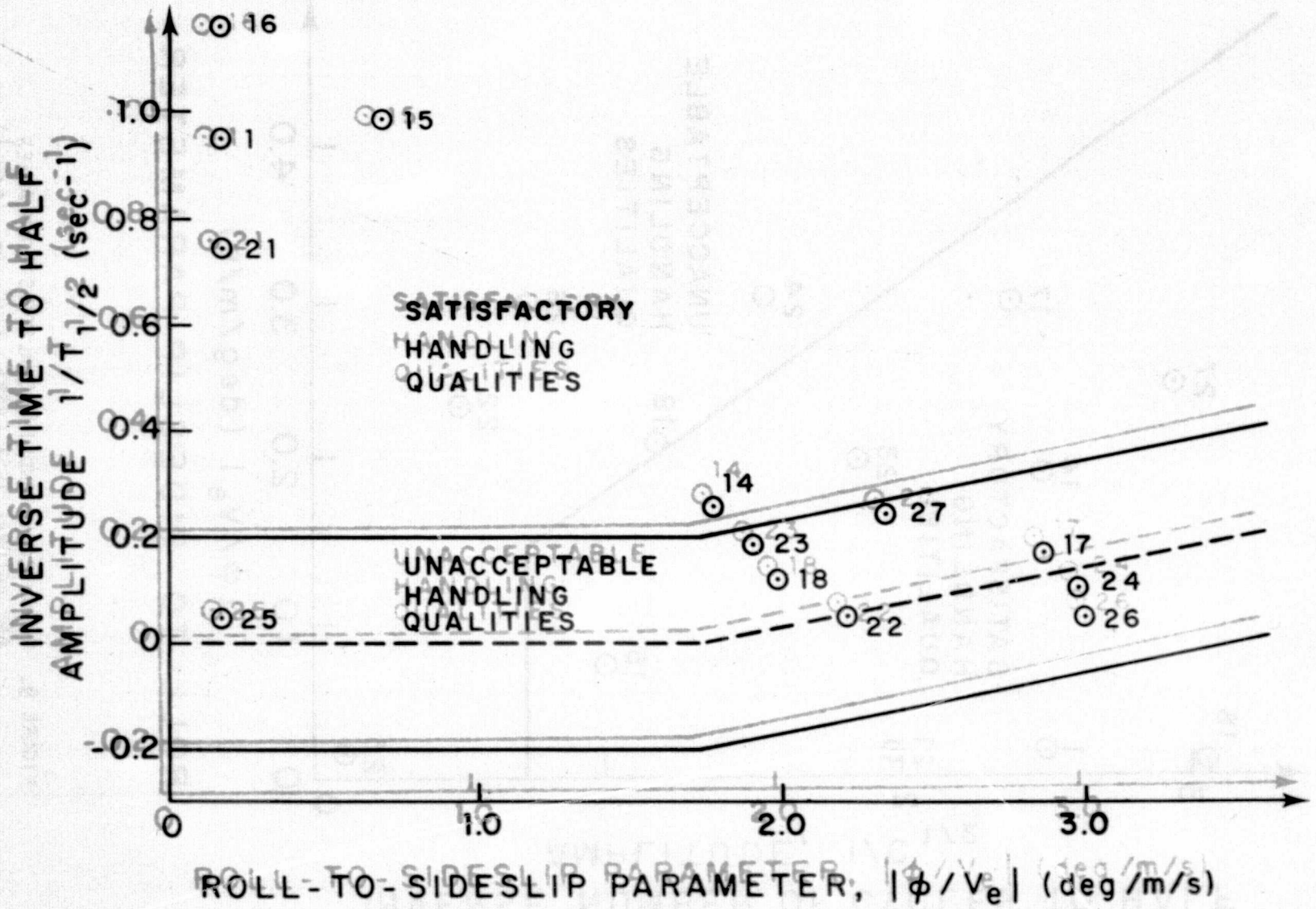

FIGURE 10. DUTCH ROLL HANDLING QUALITIES BOUNDARIES AND LATERAL TEST CASES ($1/T_{\frac{1}{2}}$ vs. $|\phi/v_e|$)

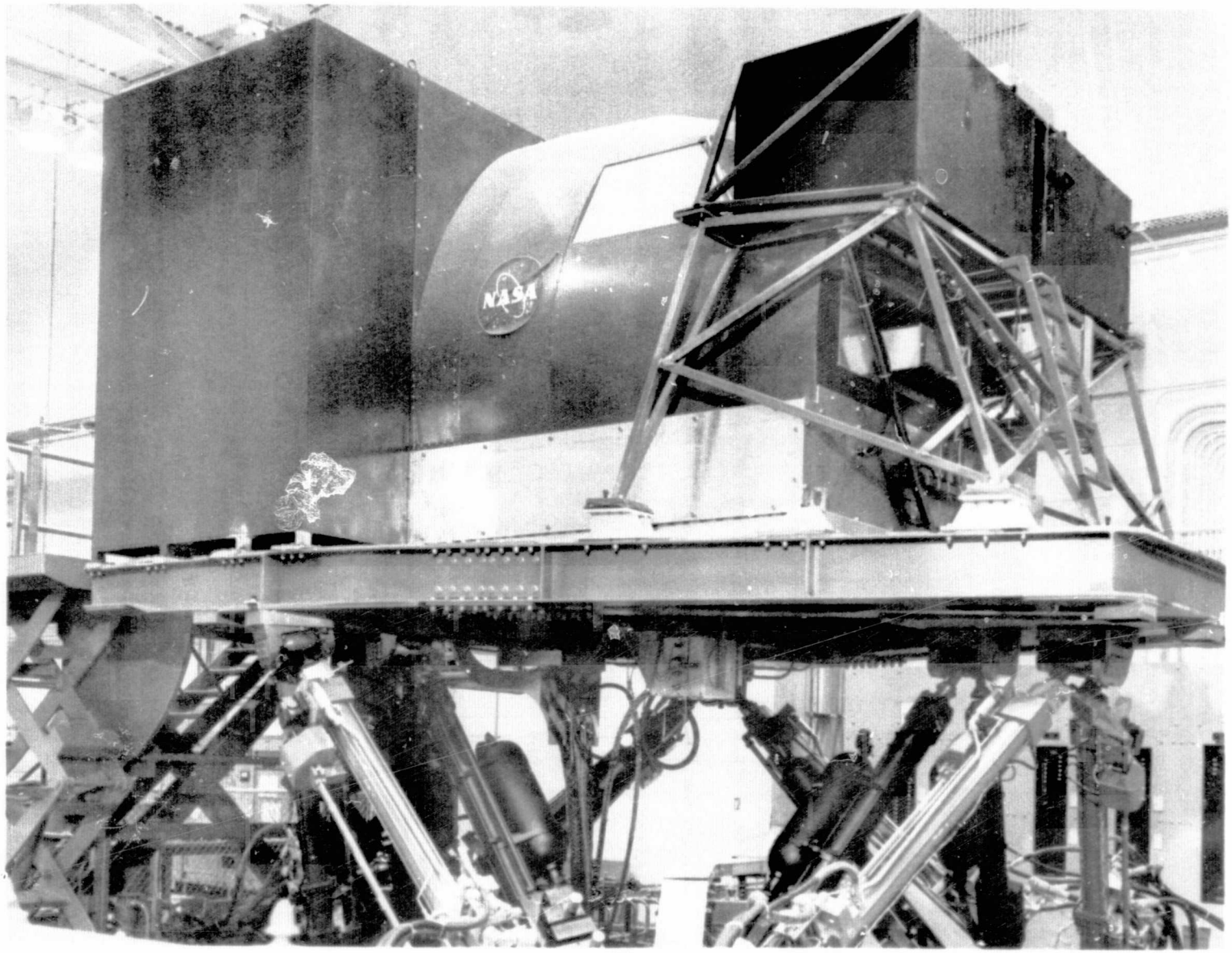

FIGURE 11. THE VISUAL MOTION SIMULATOR (VMS) AT THE NASA LANGLEY RESEARCH CENTER

the simulator, its control systems, and its data output capabilities is presented in Figure 13. A CDC-6600 digital computer, used exclusively to operate the real-time simulators at NASA Langley, was programmed with the aircraft flight conditions, stability derivatives, six-degree-of-freedom differential equations of motion, Dryden gust model, a routine for computing rms values for 22 parameters, and a simulator washout routine. The program integrates the nonlinear six-degree-of-freedom equations of motion 32 times a second to describe the motion of the real aircraft as a function of time. These values are used by the simulator washout routine to determine the position of the simulator's six moveable legs as a function of time, providing motion sensations to the occupants aboard the simulator. Due to the limited displacement of the simulator legs, and the dynamic characteristics of the hydraulic actuators, the simulator is not capable of producing the magnitude and duration of displacements, velocities, and accelerations of the real aircraft. It is the purpose of the washout routine to appropriately scale down the predicted motions of the real airplane to values which the simulator can produce without exceeding one or more of its design limits. The washout routine also attempts to drive the simulator legs back to their neutral position following a disturbance from equilibrium in anticipation of a future disturbance. This "centering" routine is to allow for maximum displacement during some future motion, and the motion due directly to this portion of the routine is designed to be of such magnitude that it be subliminal to the simulator occupants (18). (Time constants of five seconds or greater are characteristic of such motions.)

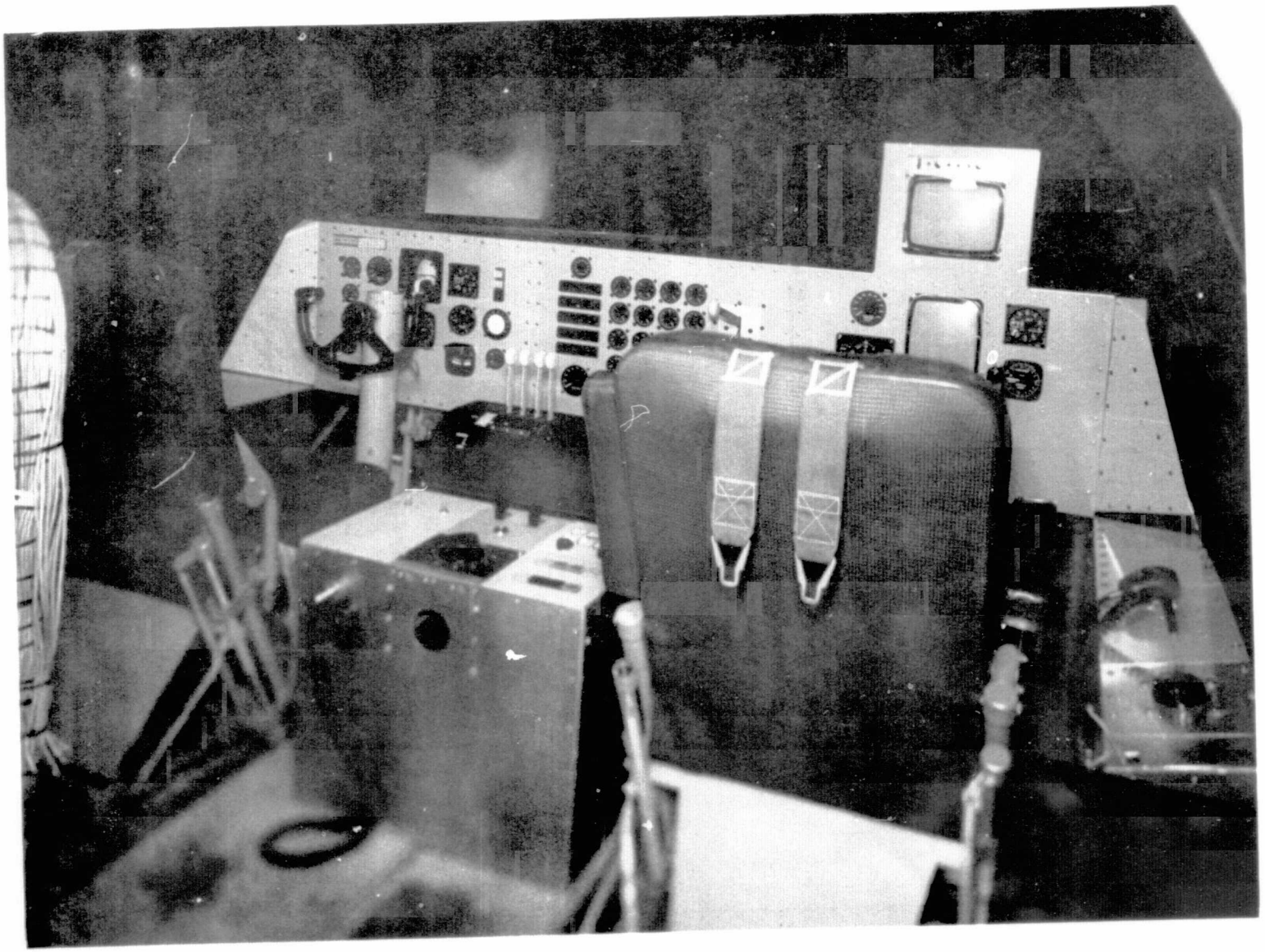

FIGURE 12. INTERIOR CABIN OF THE VISUAL MOTION SIMULATOR

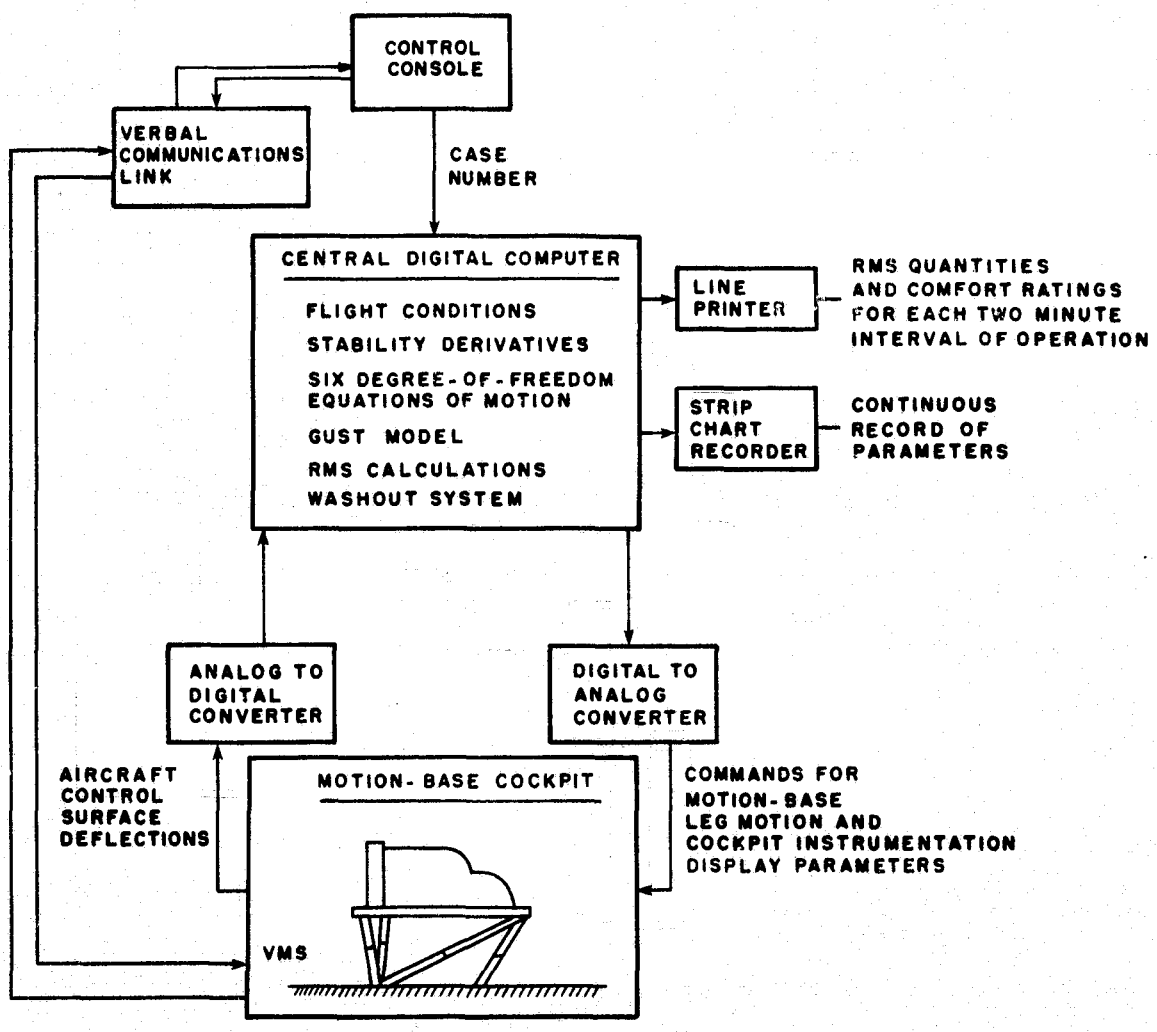

FIGURE 13. BLOCK DIAGRAM OF MOTION-BASE SIMULATOR APPARATUS

A detailed description of the physical dimensions and the performance specifications of the VMS may be found in References (18), (19), and (20). For all tests the pilot was to perform an instrument flight rules (IFR) task and was given no visual or "out-the-window" cues. This condition was chosen to provide the pilot with a representative workload of cockpit duties and, at the same time, somewhat simplify the simulation. A ride-quality subject with past experience using the U.Va.-developed 5-point ride-quality rating scale and actual in-flight ride-quality evaluation experience rode aboard the simulator with the pilot to evaluate the ride quality of each configuration. Like the pilot, the ride-quality subject was given no visual cues, and the flight instruments in front of him were covered. The pilot used in the simulations was a fully instrument-rated pilot with over 3000 hours of flight time.

The 27 test cases were run in random order three times each, with each test run lasting 16 minutes. Each 16-minute segment consisted of the following subsegments. For the first 10 minutes, the pilot is instructed to fly straight and level. During this time, the ride-quality subject on board the simulator evaluates the ride quality every two minutes. For the next two minutes, the pilot executes a two-minute turn in which the aircraft changes heading by 180^{o}, descending 304.8 m (1000 feet) for the first minute and climbing 304.8 m (1000 feet) to the original altitude in the second minute. The ride-quality subject evaluates the ride of this two-minute segment. The pilot is then asked to execute a second two-minute turn, identical to the first, and return to the original aircraft heading. Again, the ride-quality

subject evaluates the ride of this segment. In the final two minutes of each run, the pilot is instructed to separately pulse the elevator, aileron, and rudder to enable him to better evaluate the handling qualities of the particular configuration being investigated. Simultaneously, the ride-quality subject evaluates the comfort levels of the motions produced by each of the control pulses. For the study at hand, only the ride-quality evaluations taken during the straight and level portions of each run will be used for analysis. Evaluations taken during the turns and control pulses are recorded for possible future use. Following the run, the pilot is asked to complete a questionnaire rating his ability to maintain straight and level flight, and give his opinion of the overall handling qualities of the case being studied using the Cooper-Harper rating scale (21). The Cooper-Harper scale is a 10-point rating scale used by test pilots to quantify pilot opinion of aircraft handling qualities, with 1 being most desirable and 10 being almost unflyable. Also, the ride-quality subject is asked to give an overall rating of the ride quality of the cruise portion of this configuration. Samples of the rating forms used by the pilot and subjects are presented as Figures 14 and 15.

During each run, continuous strip-chart recordings are made displaying time histories of various aircraft parameters. These include the three linear accelerations and three angular rates of the aircraft in the body axes, elevator, aileron, and rudder deflections, throttle position, altitude, rate of climb, airspeed, and heading, as well as a time channel indicating the times when ride-quality responses are taken. A sample output is shown in Figure 16.

Date_____ Case Number_____

Rate the following using the Cooper-Harper scale:

Your ability to maintain straight and level flight _____

Your opinion of overall handling qualities _____

Do you have any particular comments regarding the handling qualities of this configuration?

Cooper-Harper Scale

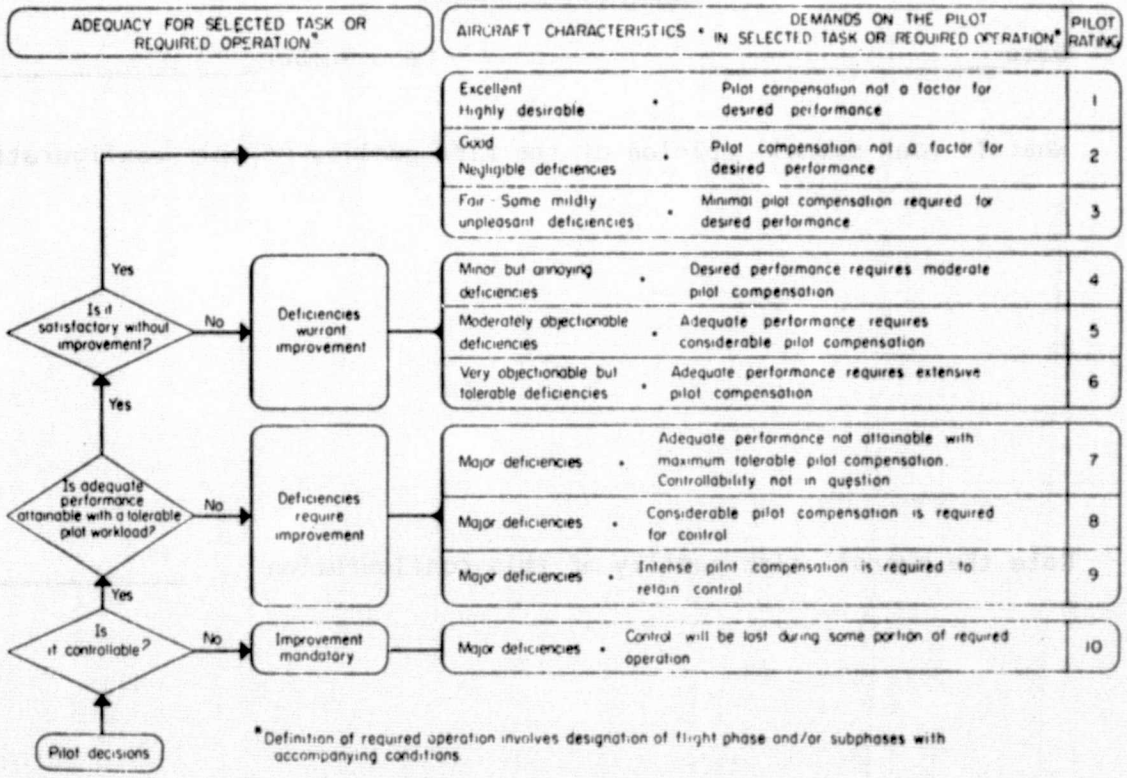

*Definition of required operation involves designation of flight phase and/or subphases with accompanying conditions.

FIGURE 14. EVALUATION PILOT'S HANDLING QUALITIES RATING SHEET

Date_____ Case Number_____

What is your overall opinion of the ride quality of this configuration?

Rate the overall ride quality of this configuration _____

Date_____ Case Number_____

What is your overall opinion of the ride quality of this configuration?

Rate the overall ride quality of this configuration _____

FIGURE 15. RIDE-QUALITY TEST SUBJECT'S RATING SHEET

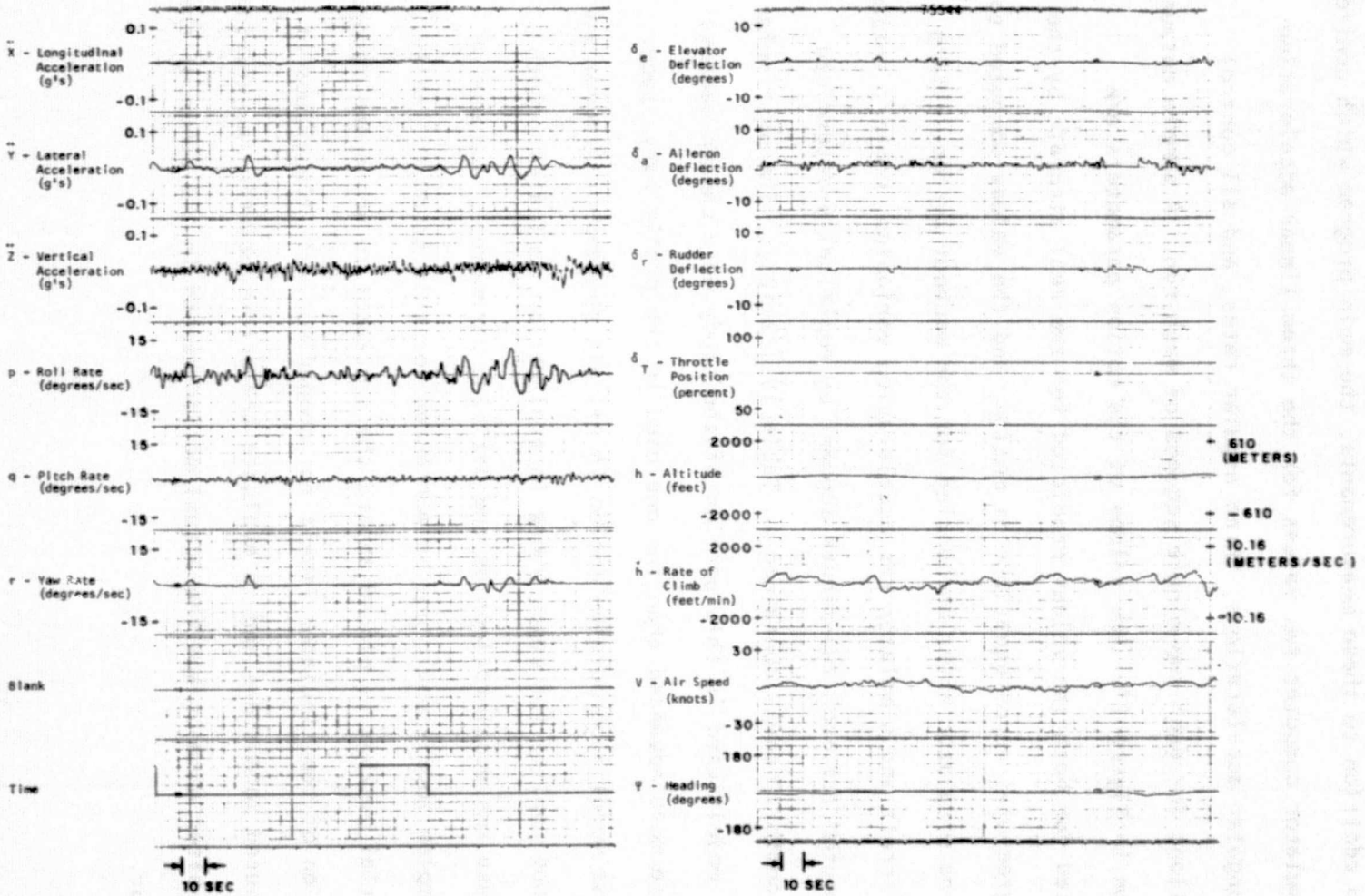

FIGURE 16. TYPICAL STRIP-CHART OUTPUT OF FLIGHT PARAMETERS
(LEVEL FLIGHT, σ = 1.524 m/sec (5 fps))

In addition to these measurements, the main program which controls the simulator computes rms values for the three linear accelerations, three angular accelerations, three angular rates, and all control deflections for each two-minute segment of each run. A sample output is shown in Figure 17. Rms values of the motion parameters are evaluated for both the values predicted for the real aircraft by the six-degree-of-freedom equations of motion, and the values computed to drive the simulator after accounting for the washout system. Using real aircraft and simulator rms acceleration variables, comfort ratings are computed for each two-minute segment by empirically-determined linear comfort models contained in Table IV (22)(23). The particular comfort models used in this portion of the study were chosen because they were more advanced than the one used in the preliminary study. The first model incorporates motion in all six degrees-of-freedom and the second applies for cases where lateral motion dominates. Both models use rms accelerations as the defining parameters, and use of more complex models would not be warranted for this study. Finally, an inertial package is placed aboard the simulator to sense and record the motion of the simulator itself for comparison with the values of the computed parameters and to evaluate the errors between the driving signals after washout and the actual motion sensed in the cabin of the simulator.

CASE NO. 17 RUN NO. 6 DATE 08/27/74

	UDOT(G)	VDOT(G)	WDOT(G)	P(RD/SEC)	Q(RD/SEC)	R(RD/SEC)	PDOT(R/S2)	QDOT(R/S2)	RDOT(R/S2)	C.R.
	DEL E	DEL A	DEL R	DEL T						
PREDICTED	.02326	.08358	.06506	.05456	.01280	.02055	.08314	.04359	.01948	4.17
ACTUAL	.01181	.03584	.00816	.01947	.00567	.00835	.03441	.02244	.00933	2.72
	1.13917	.88472	.34901	5.86934						
PREDICTED	.01582	.05199	.05837	.03526	.01254	.01004	.07536	.04409	.00963	3.46
ACTUAL	.00786	.02248	.00884	.01479	.00571	.00451	.03908	.02267	.00493	2.44
	1.23218	.57127	.16260	5.86935						
PREDICTED	.01523	.07554	.06666	.05560	.01332	.01647	.07194	.04538	.01681	4.02
ACTUAL	.00812	.02904	.00877	.01813	.00595	.00697	.03208	.02328	.00851	2.58
	1.26407	.66390	.28698	5.83675						
PREDICTED	.02023	.07469	.05597	.04612	.01207	.01527	.07071	.04030	.01911	3.91
ACTUAL	.00976	.03021	.00836	.01631	.00538	.00685	.03254	.02083	.00961	2.60
	1.10836	.77486	.31523	5.85183						
PREDICTED	.02217	.06345	.07984	.03971	.01619	.01411	.07722	.05202	.01385	3.87
ACTUAL	.01109	.02581	.00851	.01648	.00692	.00592	.03663	.02644	.00721	2.51
	1.27205	.67816	.24194	5.88659						
PREDICTED	.04868	.14111	.15450	.06693	.02655	.03681	.15890	.07254	.03508	6.10
ACTUAL	.02466	.05514	.00888	.03101	.00953	.01276	.06232	.03622	.01614	3.12
	1.32233	1.88327	.67374	5.82328						
PREDICTED	.05705	.14326	.12277	.08741	.02207	.04725	.13175	.05579	.03915	5.89
ACTUAL	.02685	.05485	.00825	.03108	.00810	.01700	.04983	.02816	.01768	3.11
	.92308	1.64073	.82524	5.99040						
PREDICTED	.03957	.14691	.26218	.09207	.04421	.03643	.15764	.08039	.03033	5.84
ACTUAL	.02306	.04503	.01001	.02062	.01414	.00912	.04786	.03559	.01000	2.92
	1.71015	2.07675	.55912	5.70115						

FIGURE 17. TYPICAL COMPUTER OUTPUT OF RMS MOTION VARIABLES AND PREDICTED COMFORT RATINGS

TABLE IV

COMFORT MODEL

$$CR = 1.85 + 11.5\, a_N + 5.7\, a_T + 1.0\, a_L + 0.2\, a_{ROLL} + 0.2\, a_{PITCH} + 1.5\, a_{YAW} \qquad (a_N \geq 1.6\, a_T)$$

$$CR = 1.9 + 8.1\, a_N + 20.9\, a_T \qquad (a_N < 1.6\, a_T)$$

where

a_N = normal rms acceleration (g's)

a_T = transverse rms acceleration (g's)

a_L = longitudinal rms acceleration (g's)

a_{ROLL} = rms angular acceleration about X body fixed axis (radians/sec^2)

a_{PITCH} = rms angular acceleration about Y body fixed axis (radians/sec^2)

a_{YAW} = rms angular acceleration about Z body fixed axis (radians/sec^2)

CR = comfort rating where:

1 - very comfortable

2 - comfortable

3 - neutral

4 - uncomfortable

5 - very uncomfortable

CHAPTER IV

RESULTS AND CONCLUSIONS

From the data collected on the VMS, several statistical quantities were computed for each separate test case, i.e., each unique set of stability derivatives and aircraft handling qualities. Computed were means and standard deviations of the comfort ratings of each test case. These quantities were found for the comfort ratings predicted for the actual aircraft, the ratings predicted based on the actual simulator motion, and the comfort ratings elicited from the test subjects riding aboard the simulator. These quantities are tabulated in Table V. Also, typical power spectra of the three linear accelerations obtained from measurements made by the inertial package placed aboard the simulator are presented in Figures 18, 19, and 20. The rms acceleration quantities obtained from this inertial package agreed within 10% of those computed for the simulator after washout by the central computer, indicating the computer-generated quantities were valid. Only the values computed and recorded during the straight and level portions of each simulator run were used when computing these statistics since it is the ride quality during the cruise portion of flight which is of primary interest in this study. Thus each mean and standard deviation is based on 15 data points since each test case was run three different occasions, and five ride-quality measurements were taken during the 10 minutes of straight and level flight of each run.

Comparing the mean comfort ratings for the 27 test cases as computed from the equations of motion of the real aircraft with the

TABLE V

MEAN AND STANDARD DEVIATION OF COMFORT RATINGS FOR TEST CASES (n = 15)

Case Number	Based on Predicted Real Aircraft Motion		Based on Simulator Motion		Actual Subjective Response	
	CR	σ(CR)	CR	σ(CR)	CR	σ(CR)
1	2.70	.13	2.03	.04	2.00	.00
2	2.97	.12	2.13	.08	2.07	.26
3	2.71	.13	2.11	.08	2.00	.38
4	2.91	.13	2.10	.10	2.00	.00
5	2.53	.10	2.08	.08	2.27	.46
6	2.88	.08	2.07	.05	2.13	.35
7	3.60	.62	2.06	.04	2.00	.00
8	2.64	.05	2.09	.08	2.00	.00
9	2.60	.14	2.11	.08	2.00	.00
10	2.80	.07	2.03	.05	2.07	.26
11	2.63	.06	2.09	.06	2.00	.00
12	2.57	.09	2.07	.07	2.13	.35
13	3.61	.29	2.16	.08	2.40	.51
14	3.04	.65	2.34	.16	2.33	.49
15	3.39	.09	2.17	.05	2.87	.35
16	2.93	.34	2.10	.14	2.27	.46
17	4.03	.56	2.57	.16	2.33	.49
18	4.15	.84	2.78	.32	2.40	.51
19	3.09	.16	2.05	.04	2.40	.51
20	2.67	.10	2.05	.06	2.73	.59
21	2.90	.17	2.10	.12	2.40	.51
22	4.34	.57	2.91	.26	2.33	.49
23	3.44	.72	2.48	.21	2.20	.41
24	3.97	.84	2.63	.33	2.27	.46
25	5.00	.00	2.28	.09	2.47	.52
26	4.23	.86	2.72	.28	2.47	.52
27	2.79	.15	2.22	.07	2.27	.46

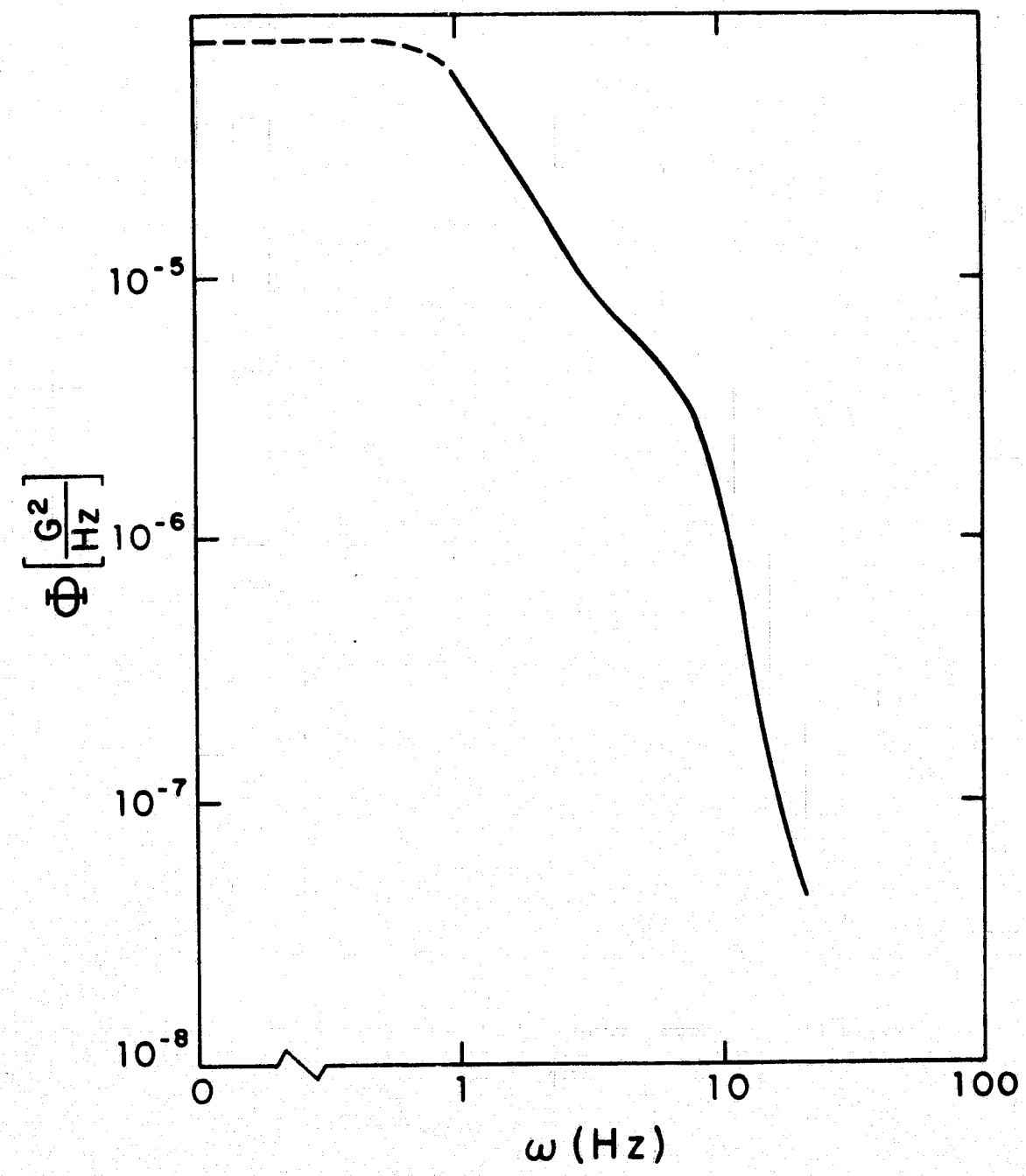

FIGURE 18. REPRESENTATIVE POWER SPECTRA OF VERTICAL ACCELERATION

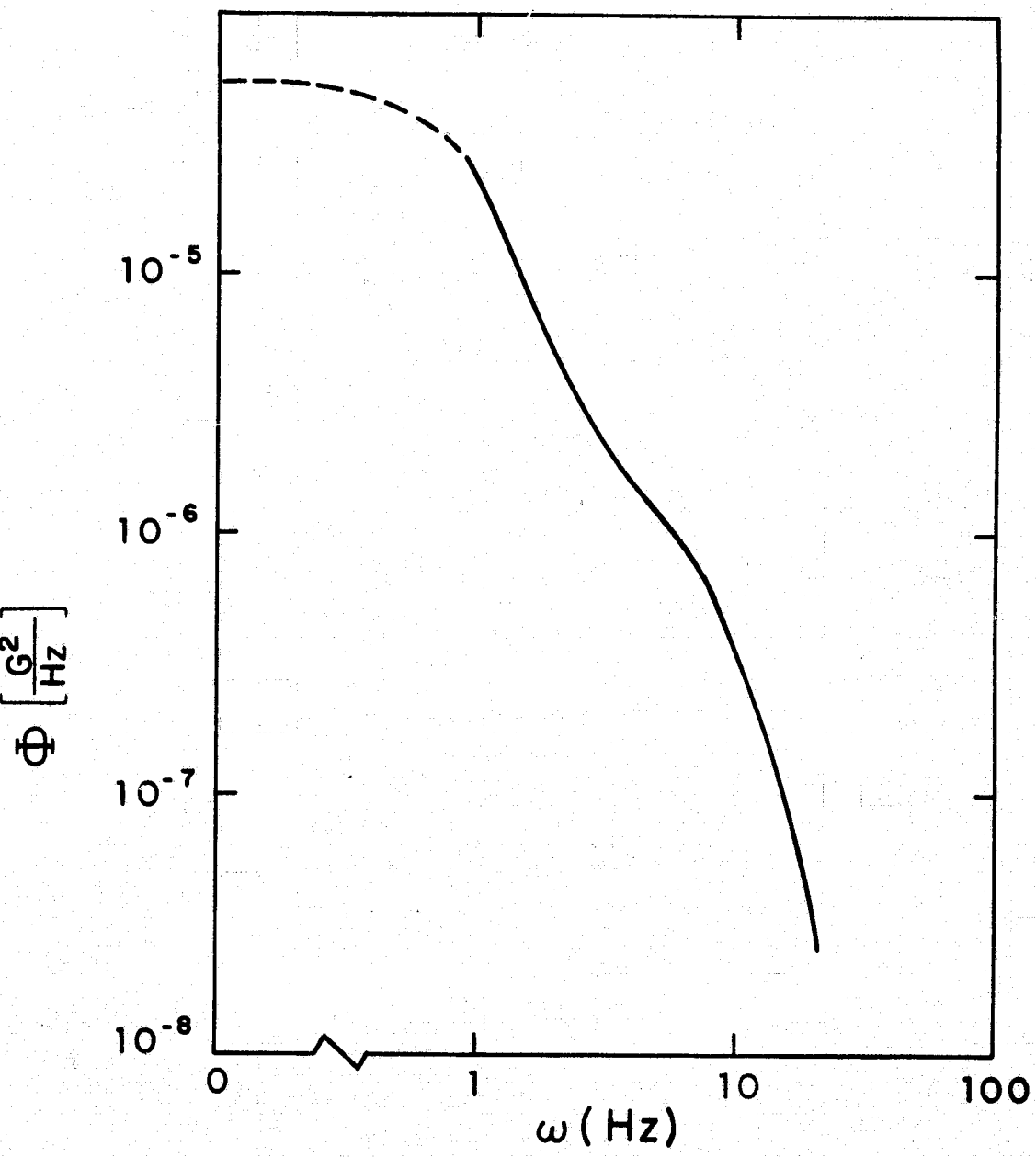

FIGURE 19. REPRESENTATIVE POWER SPECTRA OF TRANSVERSE ACCELERATION

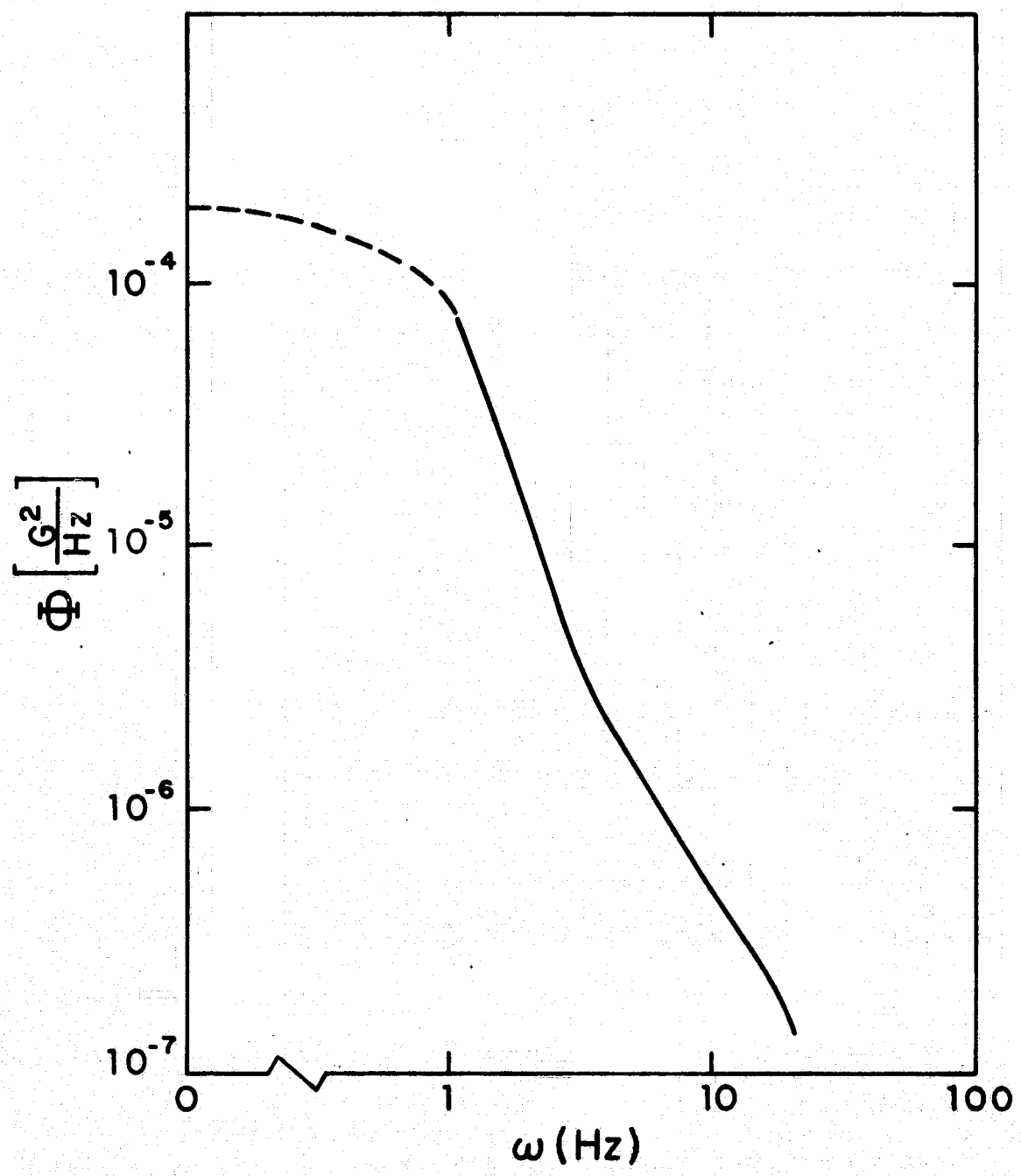

FIGURE 20. REPRESENTATIVE POWER SPECTRA OF LONGITUDINAL ACCELERATION

ratings based on the commands to actuate the simulator motion, one finds very little agreement between these two quantities (see Table V). These results are due to the physical limitations of the motion-base cockpit and the corresponding washout routine which controls the movement of the simulator's six moveable legs. This implies that the VMS was not capable of reproducing the ride quality of a given aircraft configuration on a one-to-one basis for the present study. This is, of course, due to the washout system and the displacement, velocity, and acceleration limits of the simulator. The correlation coefficient as computed by

$$r = \frac{\frac{1}{n-1} \sum_{i=1}^{n} (x_i - \bar{x})(y_i - \bar{y})}{\sigma_x \sigma_y}$$

between these two quantities is r = 0.75 however, indicating that although the motion is not being exactly reproduced as intended, there is a definite relation between the simulator ride quality and that of an actual aircraft.

Comparing the mean comfort ratings computed from the commands to move the simulator legs with the mean of the comfort ratings recorded by the ride-quality subjects riding aboard the simulator, one finds the agreement for most cases to be quite good (see Table V). The correlation coefficient for this data is r = 0.30. Part of the discrepancy between the two sets of mean comfort ratings may be accounted for by the fact that the comfort model used to predict comfort ratings based on rms accelerations is a continuous function while the actual rating scale as defined and used by the test subjects

is an integer scale. This also accounts for the low correlation coefficient for this data. Also the number of responses used in determining each mean was somewhat small (n = 15). In spite of these limitations, the agreement between these two suggests that the experienced ride-quality subjects were indeed responding in the "proper" (predicted) manner to the motions to which they were subjected, and further validates the empirical comfort models. This tends to support the theory that ground-based simulations for ride-quality studies may be of significant value, if the desired motions and environmental conditions being simulated are acceptably reproduced in the laboratory.

Using the previously-described transformation (22) which translates a comfort rating to the percent of the population satisfied with the ride, the satisfaction levels of the comfort predicted for the real aircraft for the cases when the longitudinal short-period handling qualities were varied, are plotted in Figure 21, superimposed upon the contours of short-period handling qualities. In a similar manner, variations in the lateral Dutch Roll mode handling qualities resulted in the satisfaction levels shown in Figures 22 and 23, plotted along with contours of accepted handling qualities for the Dutch Roll mode. From the data of Figure 21, lines of constant satisfaction level have been drawn and are shown in Figure 24 along with the contours of constant handling qualities for the longitudinal short-period mode. It is recognized from this figure that ride quality is indeed a function of the parameters which define short-period handling qualities, namely ω_{n_s} and ζ_s. Thus a trade-off exists between longitudinal handling qualities and ride quality. Hence, from a design standpoint, the

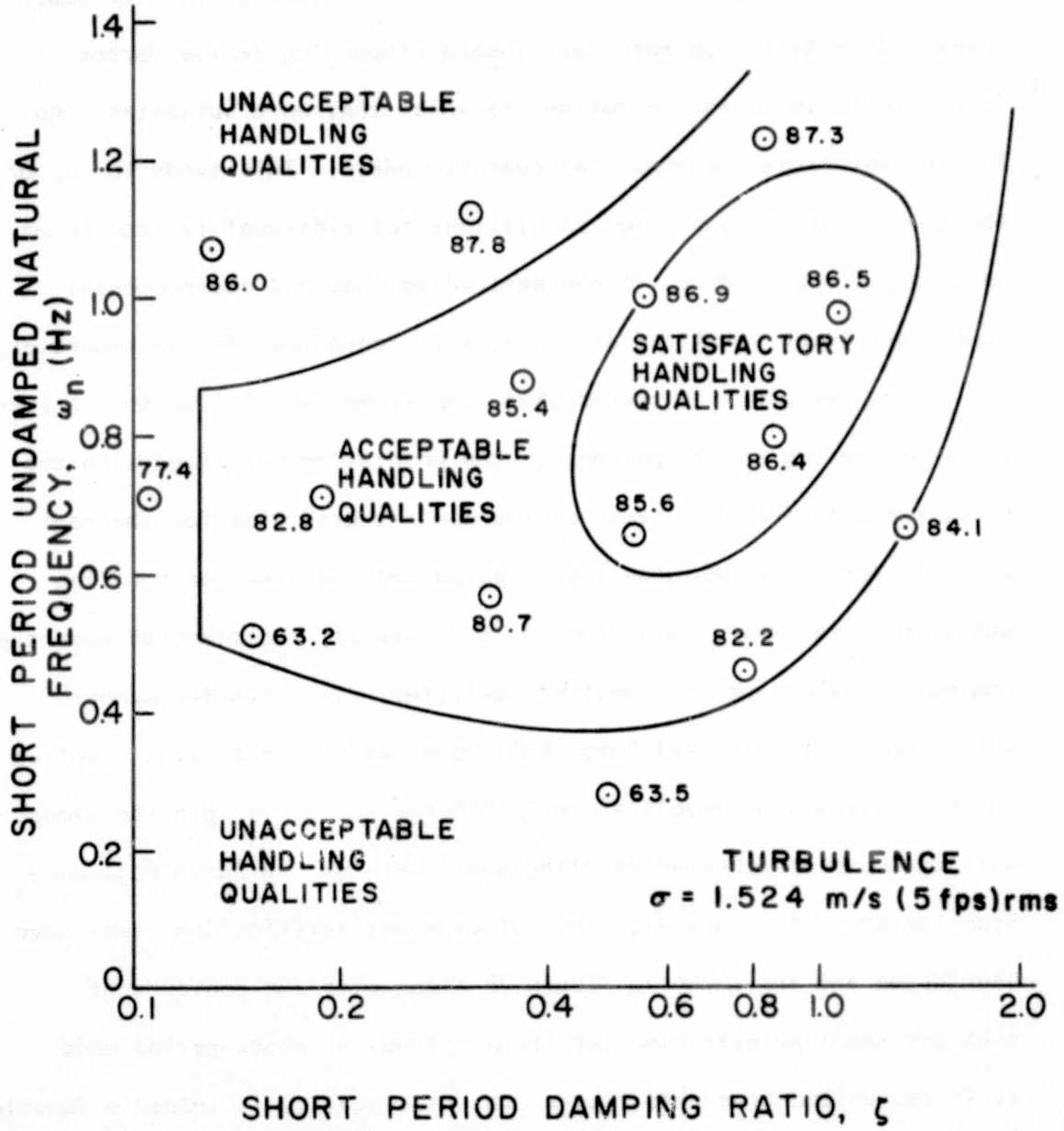

FIGURE 21. PERCENT POPULATION SATISFIED, SHORT-PERIOD HANDLING QUALITIES

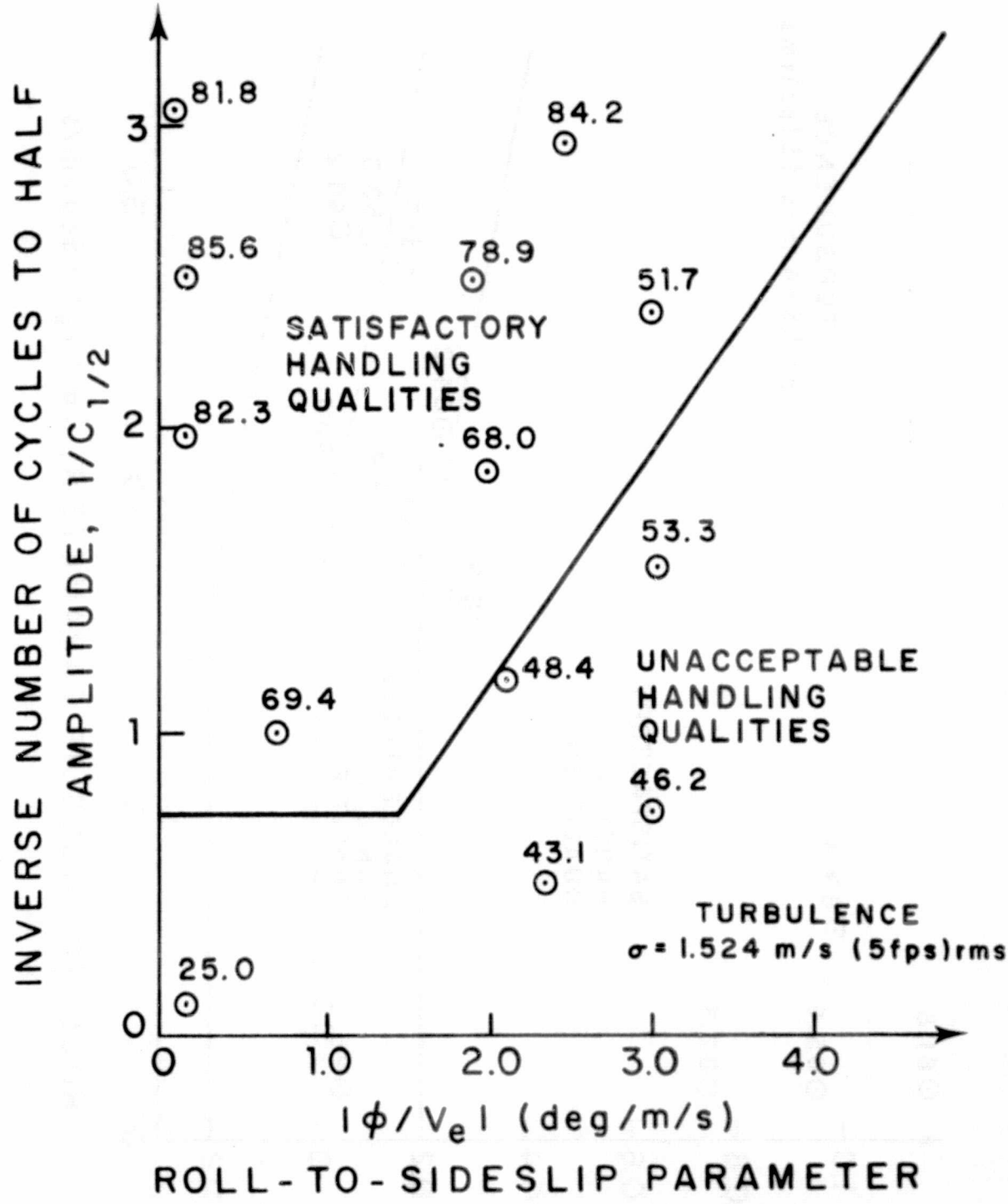

FIGURE 22. PERCENT POPULATION SATISFIED, DUTCH ROLL HANDLING QUALITIES ($1/C_{\frac{1}{2}}$ vs. $|\phi/v_e|$)

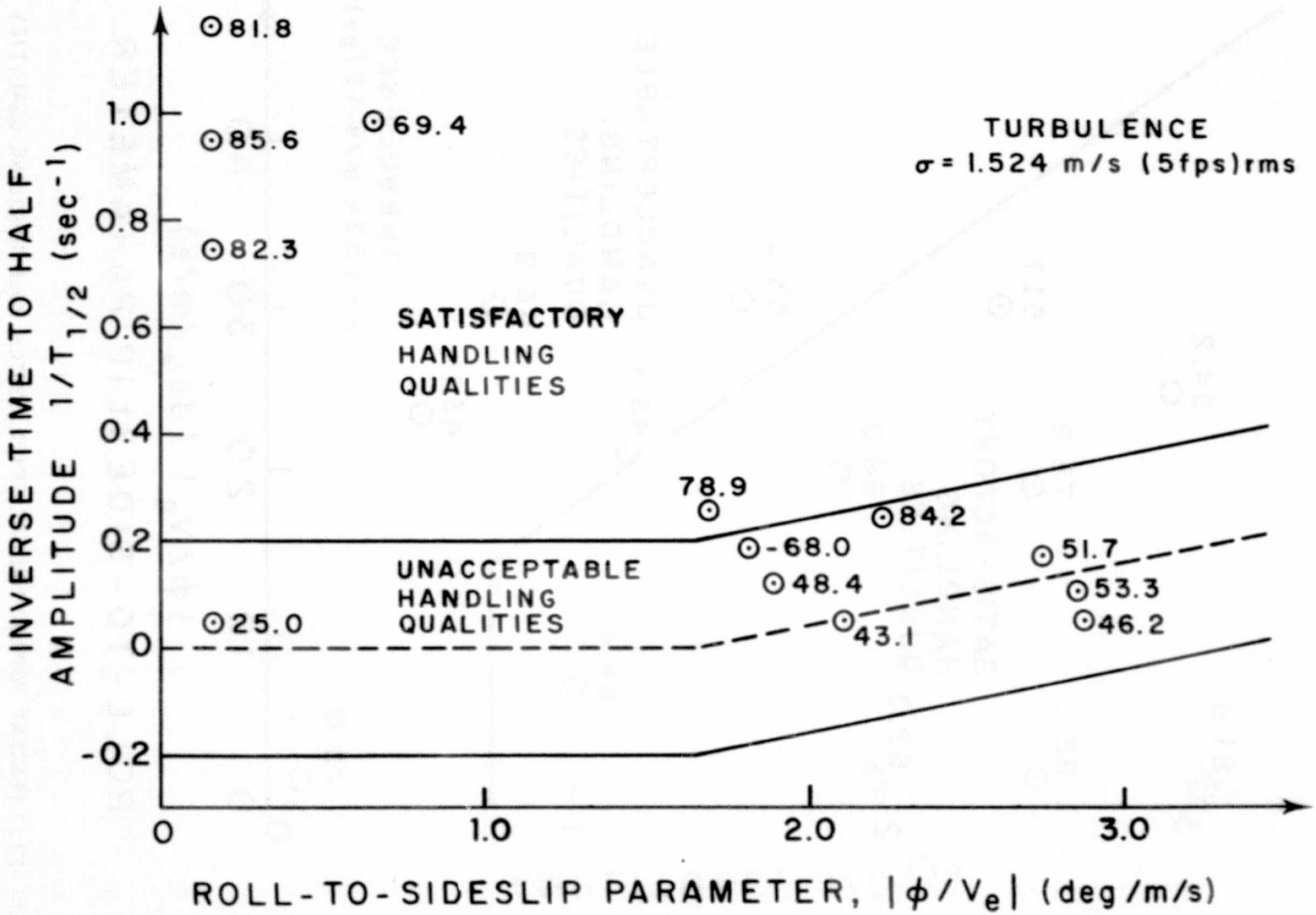

FIGURE 23. PERCENT POPULATION SATISFIED, DUTCH ROLL HANDLING QUALITIES
($1/T_{\frac{1}{2}}$ vs. $|\phi/v_e|$)

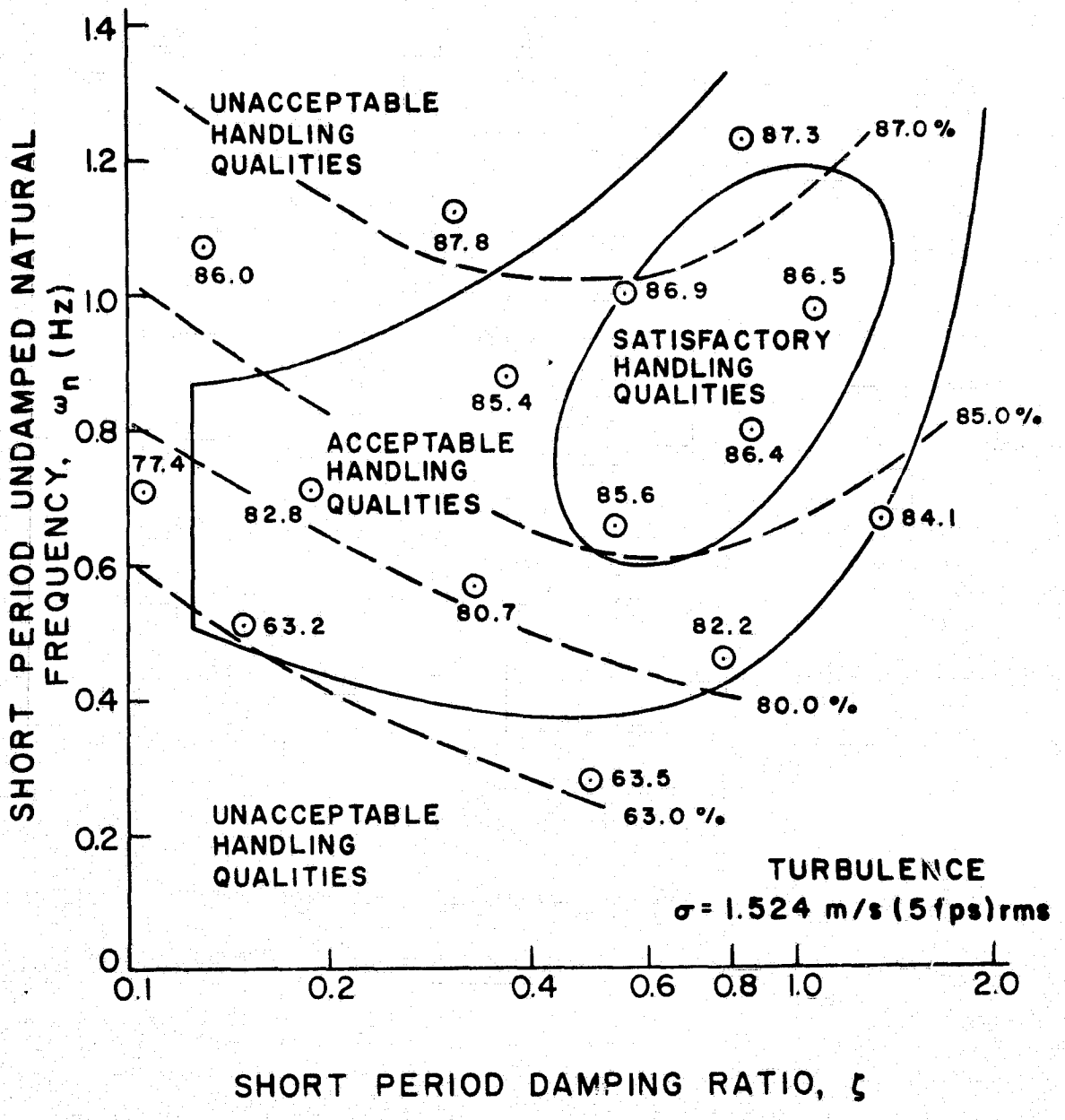

FIGURE 24. PERCENT POPULATION SATISFIED, SHORT-PERIOD HANDLING QUALITIES WITH CONTOURS OF CONSTANT SATISFACTION

designer can choose an operating point and know how both the handling qualities of the short-period mode and the corresponding level of ride quality would compare with some other design point. This would enable the designer to weigh the trade-offs between ride and handling qualities and help him make an intelligent choice of an operating point for good handling qualities and give him an idea of what level of passenger satisfaction to expect from his design.

Similarly, from Figures 22 and 23, one can identify trends of improving ride quality as defined by parameters in which lateral Dutch Roll handling qualities are defined. While it is difficult to construct contours of constant ride quality due to the sparsity of data available, the previously-observed trends hold. Namely, decreasing $C_{\frac{1}{2}_d}$, $T_{\frac{1}{2}_d}$, and $|\phi/v_e|_d$ tends to improve ride quality and raise the percentage of the population satisfied with the quality of the ride. Thus in the lateral mode, good ride quality is complimentary to good handling qualities of the Dutch Roll mode. It is worthy to note here, however, that while these regions are complimentary, there is a significant amount of variation in the percentage of passengers satisfied over the region where Dutch Roll handling qualities are judged satisfactory (68 - 85%). The designer should note here that simply designing an aircraft with satisfactory Dutch Roll handling characteristics is not all he should strive for from the ride-quality standpoint. He should realize from these figures that the further he can move his operating point away from the boundary between acceptable and unacceptable handling qualities, the more he can improve passenger satisfaction as well as improve handling qualities; he may be able to improve

passenger satisfaction by up to 20% of the total passengers carried for a design of similar wing loading and equivalent turbulence conditions as the test case. It should be re-emphasized that all the measurements taken were on one particular design, one flight condition, and one turbulence level. One would not expect the values produced by this study to be universal, applying to all conditions and turbulence levels; however, the general nature of the isocontours for ride quality and the other trends outlined should hold regardless of wing loading, turbulence level, and flight conditions.

If one takes the linearized longitudinal equations of motion for the free airplane with controls fixed, eliminates the force equation in the X body axis direction, and assumes variations in u are negligible, one obtains an approximation of the short-period mode (24). From these equations, one may develop an expression for the normal acceleration as a function of ω, the forcing frequency of an imposed sinusoidal gust oscillation. Integration over all forcing frequencies, one obtains the following relations for the rms normal accelerations as a function of the gust magnitude, $\bar{w}_g$, the short-period undamped natural frequency, ω_{n_s}, and the short-period damping ratio, ζ_s:

$$a_N \approx \frac{K_1' \bar{w}_g \, (1-k\zeta_s)^2}{\sqrt{1-\zeta_s^2}\,\omega_{n_s}} \qquad \zeta_s < 1$$

$$a_N \approx \frac{K_2' \bar{w}_g}{\omega_{n_s}} \qquad \zeta_s = 1$$

$$a_N \approx \frac{K_3 \bar{w}_g (1-k\zeta_s)^2}{\sqrt{\zeta_s^2-1}\ \omega_{n_s}} \qquad \zeta_s > 1$$

where K_1, K_2, K_3, and k are constants. Derivation of these relations may be found in Appendix E.

These relations, while derived by using the assumptions of controls fixed and allowing only sinusoidal variations in gust velocities, exhibit the contours found experimentally. Holding ζ_s constant, these equations all predict that as the short-period undamped natural frequency ω_{n_s} is increased, a_N is decreased resulting in an increase in passenger satisfaction. Similarly holding ω_{n_s} constant, a_N is decreased as ζ_s increases below $\zeta_s = 1$, predicting an increase in satisfaction for $\zeta_s < 1$. Also, a_N is increased as ζ_s increases above $\zeta_s = 1$ predicting a decrease in satisfaction for $\zeta_s > 1$. These trends agree with those observed experimentally in Figure 24.

The effect that variation of the turbulence level could have on the contours of constant ride quality may be studied using this mathematical model. For a given constant passenger satisfaction contour, the corresponding comfort rating may be found using Figure 4. The rms acceleration required to produce this level of comfort is determined from the simplified comfort model (Table II) neglecting transverse acceleration terms. Since the normal acceleration is directly proportional to rms turbulence level, one may find, by an inverse method, contours of constant passenger satisfaction for any turbulence level. For example, σ_w = 0.914 and 2.134 m/s (3 and 7 fps) result in the following satisfaction levels:

σ_w	% Satisfied			
0.914 m/s (3 fps)	89.6	88.7	86.9	82.0
1.524 m/s (5 fps)	87.0	85.0	80.0	63.0
2.134 m/s (7 fps)	83.6	82.1	72.0	44.0

These results are plotted in Figures 25 and 26. For the contours shown, passenger satisfaction varies only 7.6% for σ_w = .914 m/s (3 fps); however, for σ_w = 2.134 m/s (7 fps), passenger satisfaction varies 39.6%. Thus, for flight in regions of heavy turbulence, the selection of short-period characteristics could markedly affect the degree of passenger satisfaction.

The pilot's evaluations of his ability to maintain straight and level flight, and his opinion of overall handling qualities for all test cases are tabulated in Table VI. The pilot made several trial runs on several test cases before actual testing was begun, and these are also included in the table. This was done to let the pilot gain familiarity with the simulator, its controls and instrumentation, and use of the Cooper-Harper pilot-rating scale. The results compiled in the table contain the pilot ratings for all test cases listed in the order in which they were taken. Included are the trial run cases as well as the three test cases, during which ride-quality measurements were taken. Referring to Table VI, one can see that for most cases, the pilot was consistent among the three ratings he used to evaluate a particular case, or agreed closely on two of the three evaluations. Only on one case, number 25, did the pilot return three substantially different ratings for each test run. The final column in Table VI lists the

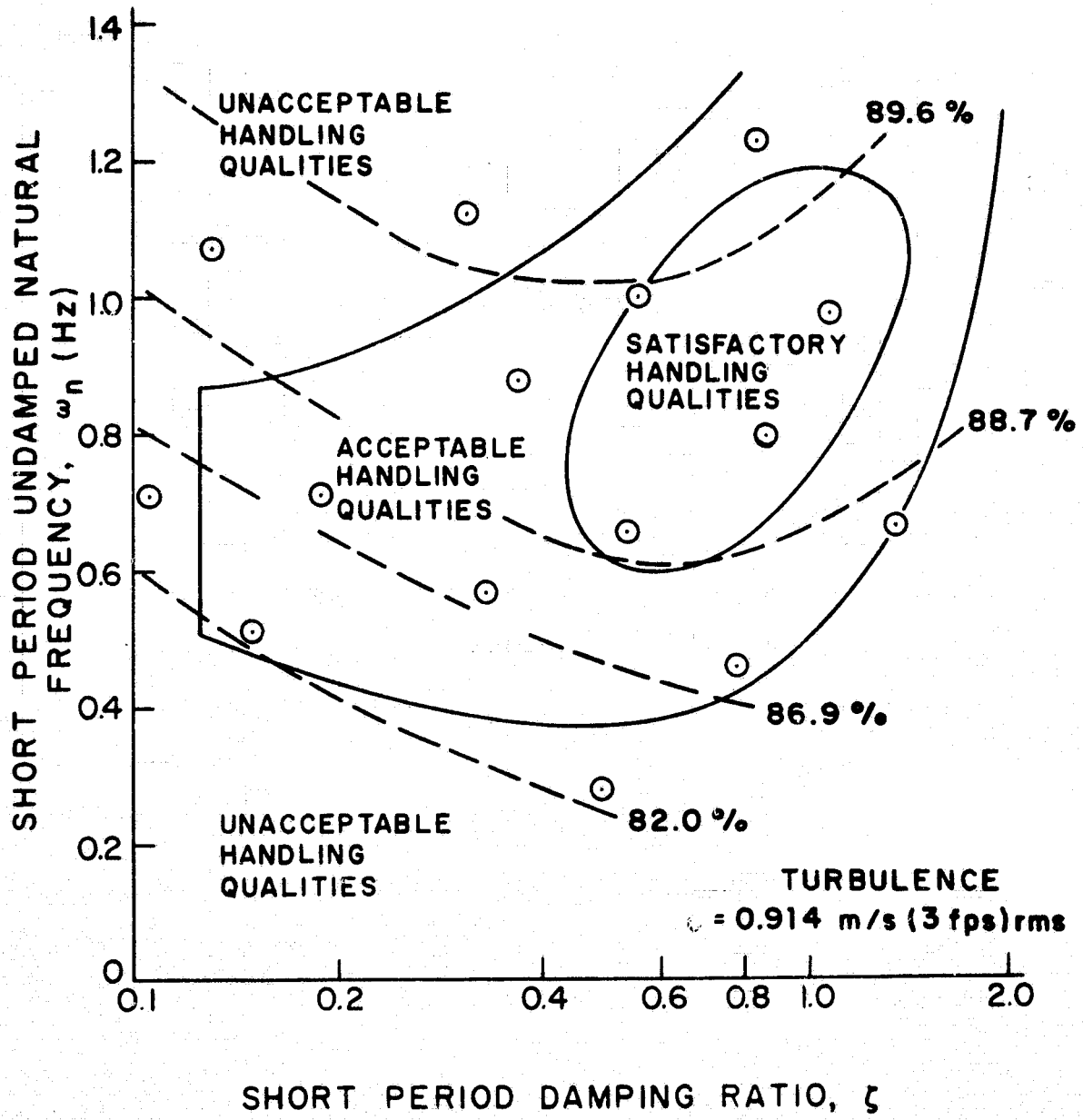

FIGURE 25. SHORT-PERIOD MODE RIDE-QUALITY VARIATIONS
σ = 0.914 m/sec (3 fps)

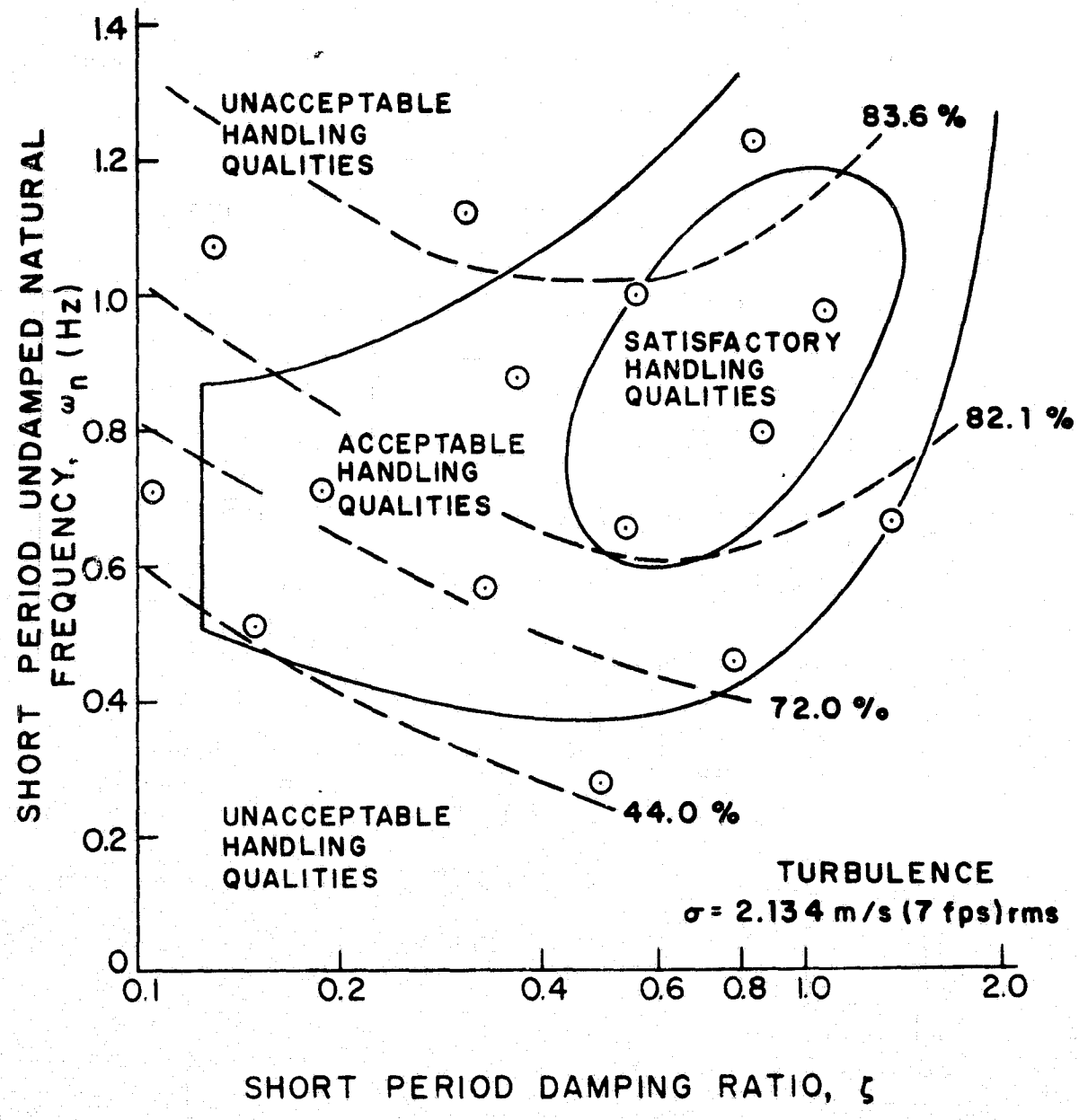

FIGURE 26. SHORT-PERIOD MODE RIDE-QUALITY VARIATIONS
σ = 2.134 m/sec (7 fps)

TABLE VI

PILOT RATINGS (COOPER-HARPER SCALE)

Case Number	Ability to Maintain Straight and Level Flight	Opinion of Overall Handling Qualities	Predicted Cooper-Harper Rating
1	3.5, 4, 2, 5, 3	3, 3.5, 2, 5, 2	3
2	4, 3, 4, 4	4, 5, 3, 4	4.5 - 5
3	2.5, 4, 7	3, 3, 7	4 - 4.5
4	3, 3.5, 4	2.5, 3, 4	6
5	4.5, 3.5, 4	3.5, 2.5, 3	7
6	5, 5, 4, 5	5, 5, 4, 6	5.5
7	6.5, 5, 7	9.5, 9, 8	8
8	2.5, 4, 4	3.5, 3, 3	2.5 - 3
9	3.5, 4, 3	3, 3, 4	3.5
10	3, 3, 3, 3, 4	7, 3, 4, 4, 4	6.5
11	1, 3, 7	2, 2, 7	2
12	2.5, 5, 4	7, 3.5, 4	4 - 4.5
13	6, 7, 7	8, 7, 6	6.5
19	6.2, 5, 7	8, 6, 7	8
20	7, 4.5, 6	7, 6, 5	8
14	7, 3, 7	8, 8, 8	5
15	3, 3, 7	6, 4, 7	6
16	2.5, 4, 4	3, 3, 3	3
17	10, 9, 9	10, 10, 10	6
18	6, 8, 9	8, 10, 10	6.5
21	3, 3, 5	2.5, 3, 3	3.5
22	9, 9, 7	10, 10, 10	9
23	10, 9, 7	10, 10, 7	6
24	9, 5, 8	10, 9, 9	7
25	7, 4, 6	10, 3, 6	8
26	10, 10, 8, 8, 10	10, 10, 10, 9, 10	9
27	6, 5, 5	9, 8, 7	5

predicted value which should be expected for each test case. These values have been determined by interpolation between the pilot opinion isocontours of Figures 8, 9, and 10 which locate the test cases in terms of their short-period and Dutch Roll handling qualities. The agreement between ratings of overall handling qualities made by the pilot with the predicted values of each case is good for some cases but not for others. The primary factor of concern here is simulator realism. The tests were run with no visual cue given to the pilot, and a limited amount of kinesthetic cues, particularly in the normal direction, due to the simulator design limits and the washout system. The average of the overall pilot ratings for the three test runs are plotted along with the established contours for short-period and Dutch Roll handling qualities in Figures 27, 28, and 29. The dotted lines on these figures indicate the handling qualities boundaries as suggested by the limited data taken in this study. While there is not exact agreement between the existing boundaries and the test data, the general trends exhibited by the two are in good agreement.

For the short-period mode, the cases with good handling qualities (ratings of 4 and less) were not as close to the predicted values as were the cases where the handling qualities were not good (ratings of 5 or more). For the Dutch Roll mode, the recorded ratings agree well with the predicted ratings for low Cooper-Harper ratings (below 4) and high Cooper-Harper ratings (above 7); however, agreement for marginal ratings (between 4 and 7) was poor.

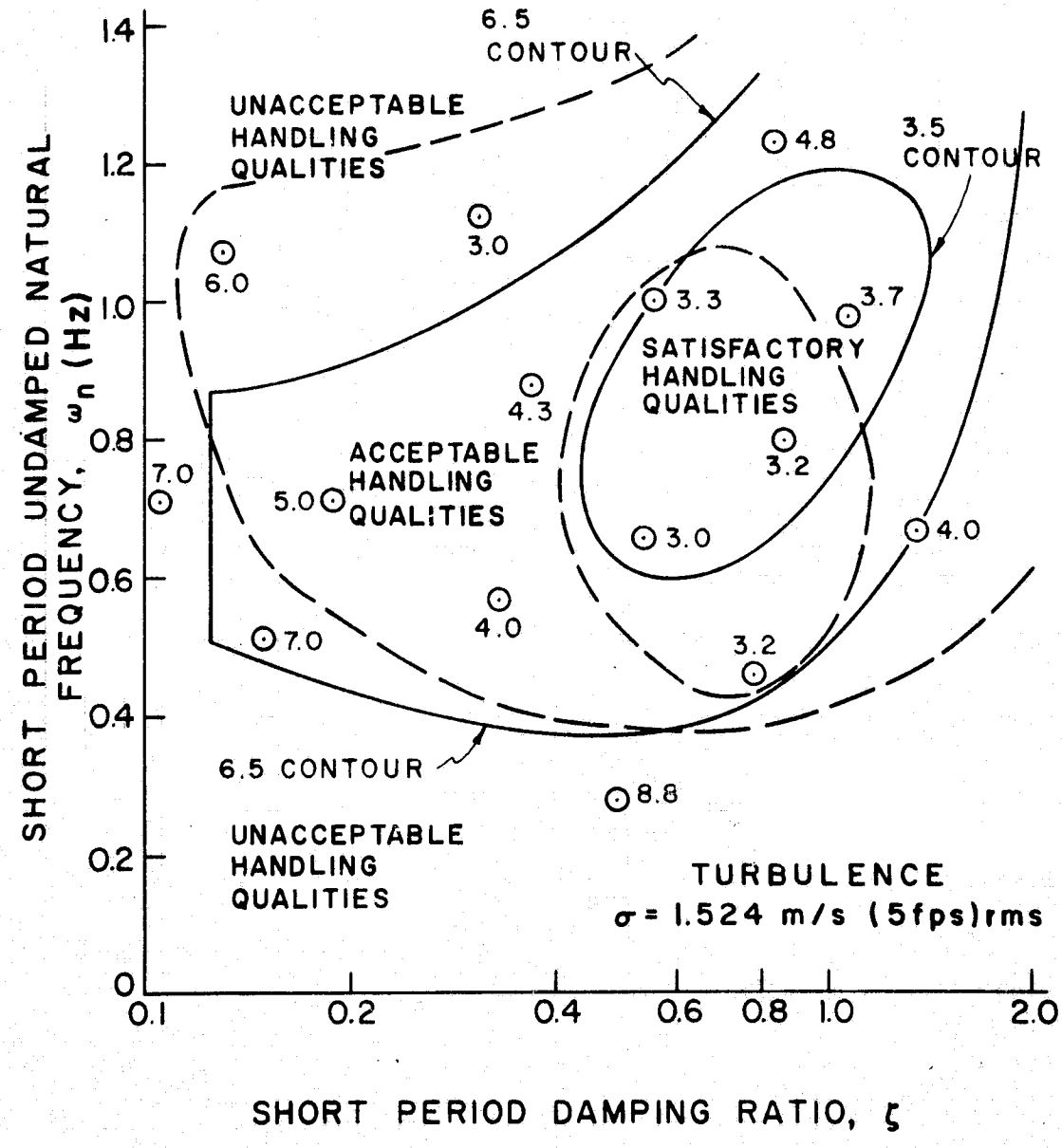

FIGURE 27. AVERAGE PILOT RATINGS, SHORT-PERIOD HANDLING QUALITIES

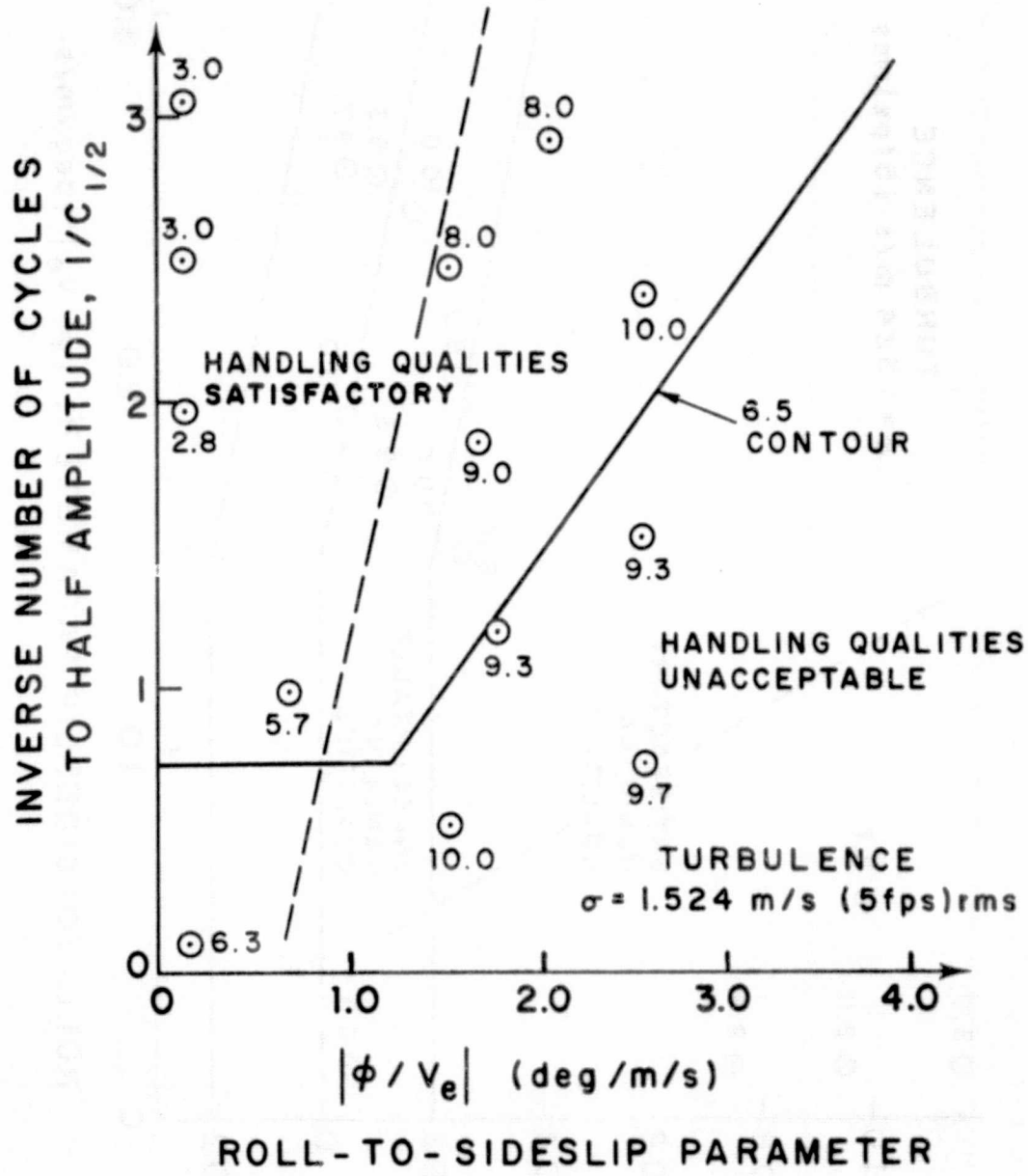

FIGURE 28. AVERAGE PILOT RATINGS, DUTCH ROLL HANDLING QUALITIES ($1/C_{\frac{1}{2}}$ vs. $|\phi/v_e|$).

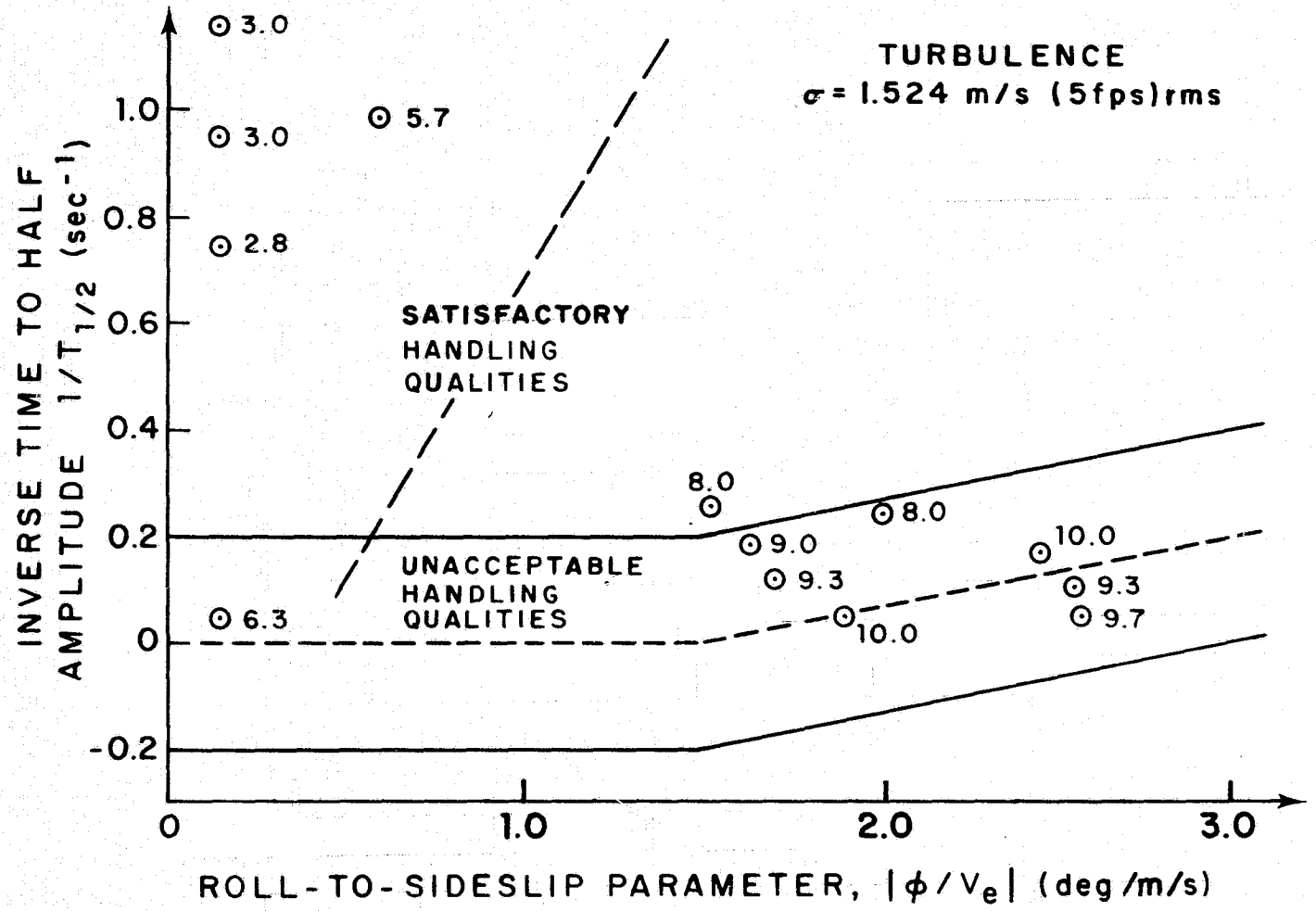

FIGURE 29. AVERAGE PILOT RATINGS, DUTCH ROLL HANDLING QUALITIES
($1/T_{\frac{1}{2}}$ vs. $|\phi/v_e|$)

Also, there appeared to be a qualitative relationship between control activity and pilot opinion of handling qualities. Figure 30 depicts the variation of elevator activity for typical cases in which the longitudinal short-period characteristics were varied. As is evidenced from these traces, average Cooper-Harper rating of handling qualities increased as greater elevator activity was required to maintain level flight. The activity of the other control surfaces remained essentially constant while the short-period characteristics were varied. Similarly, variation of the Dutch Roll mode characteristics (Figure 31) were accompanied by changes in aileron activity. Higher Cooper-Harper ratings were accompanied by increased aileron activity necessary to maintain straight and level flight. The apparent activity levels of the remaining control surfaces were constant as Dutch Roll characteristics were varied.

The only quantitative measures of control activity obtained were rms values of the control surface deflections. This measure was found to be unsatisfactory for determining control activity, due to the time averaging process involved in computing an rms of a parameter which is very small or zero for a substantial portion of the averaging period.

Also, in the case of elevator rms deflection, it was not possible to exactly determine the equilibrium elevator deflection and bias this value out of the rms calculation. Another measure of control activity should be used in the future to quantify the activity level. Such quantities as the percentage of time the control surface deflection

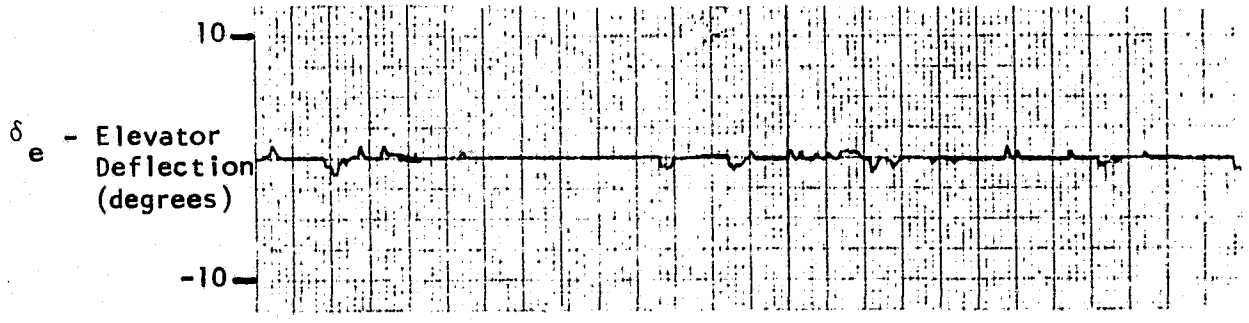

Light Activity, Case #1, Average Cooper-Harper Rating = 3.0
Predicted Cooper-Harper Rating = 3.0

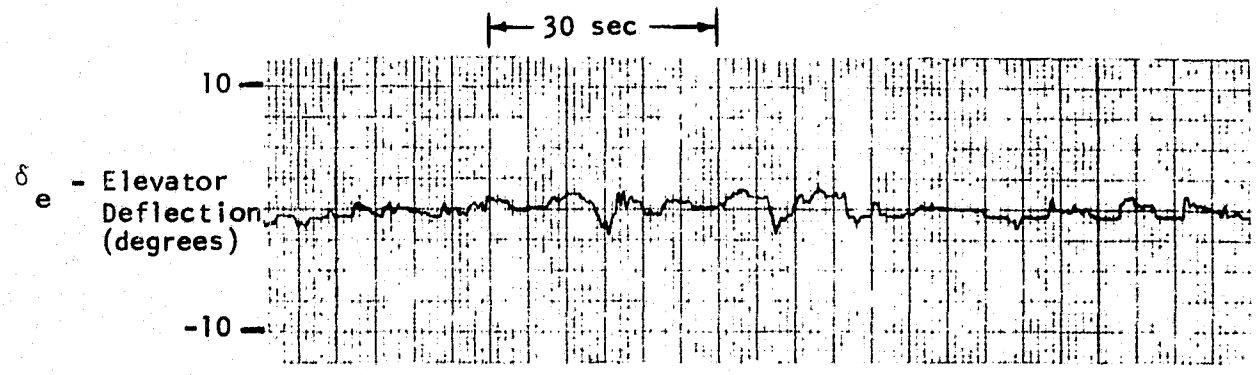

Moderate Activity, Case #6, Average Cooper-Harper Rating = 5.0
Predicted Cooper-Harper Rating = 5.5

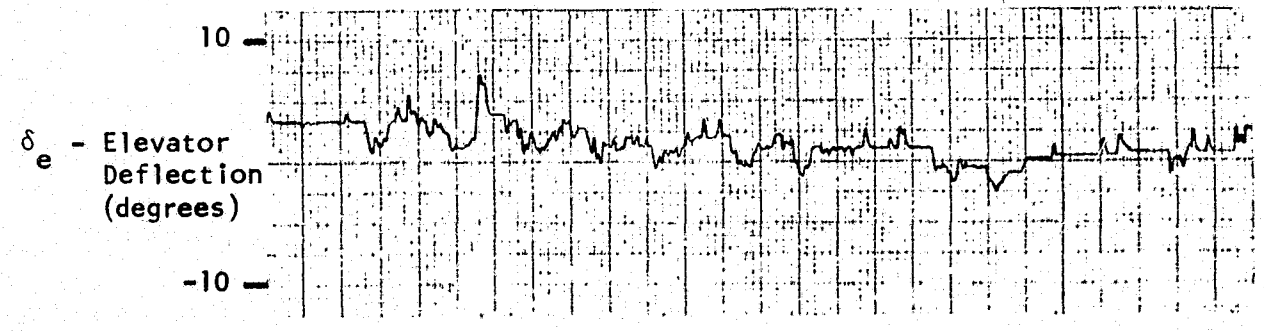

Heavy Activity, Case #20, Average Cooper-Harper Rating = 6.0
Predicted Cooper-Harper Rating = 8.0

FIGURE 30. TYPICAL ELEVATOR ACTIVITY VARIATIONS

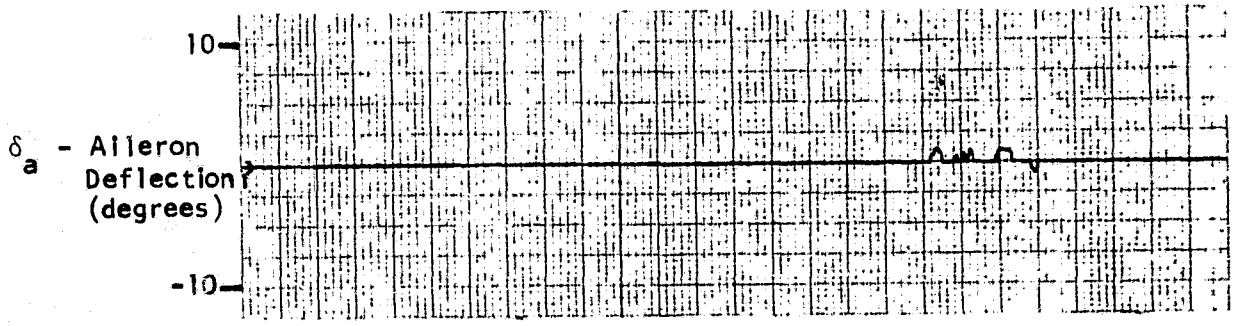

Light Activity, Case #1, Average Cooper-Harper Rating = 3.0
Predicted Cooper-Harper Rating = 3.0

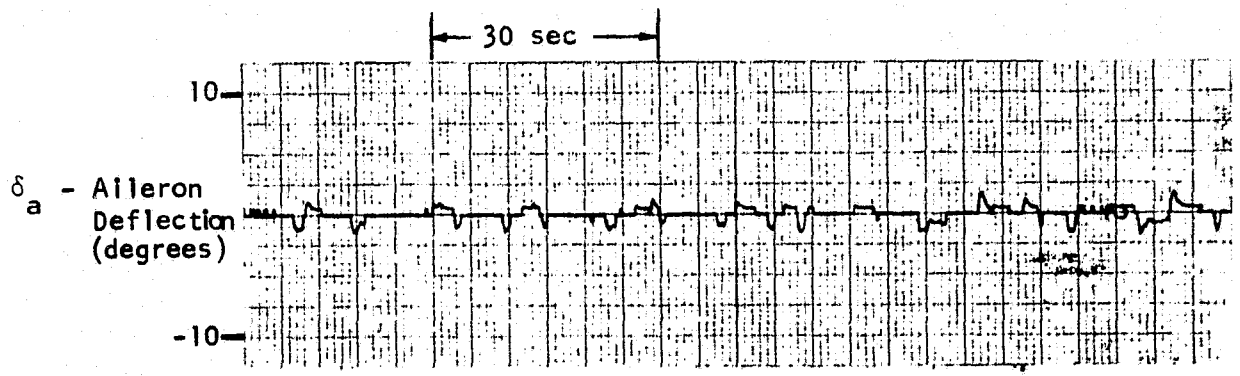

Moderate Activity, Case #15, Average Cooper-Harper Rating = 5.7
Predicted Cooper-Harper Rating = 6.0

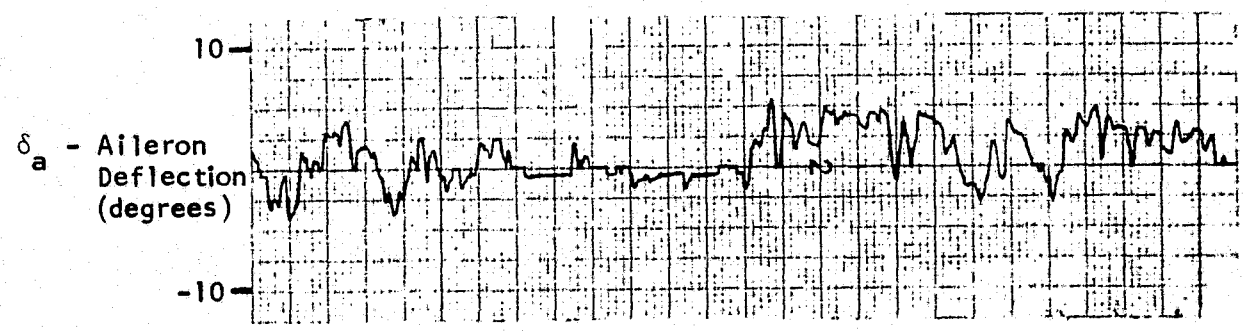

Heavy Activity, Case #26, Average Cooper-Harper Rating = 9.7
Predicted Cooper-Harper Rating = 9.0

FIGURE 31. TYPICAL AILERON ACTIVITY VARIATIONS

exceeds a specified value or the number of peaks (max or min) per unit time experienced by a control surface may be more meaningful than rms for defining control activity.

Taking the latter measure and using a 1.5^{o} threshold for both the elevator and ailerons, the total number of exceedances was determined. Figure 32 shows how elevator activity varied as the short-period handling qualities varied. As seen, this measure of pilot activity increases with undamped natural frequency and is not complimentary with the handling qualities contours. The trend implies that the pilot uses more elevator motion to maintain straight and level flight when the short-period frequencies were high, possibly because he is not physiologically able to react rapidly enough to control a disturbance. In a similar manner, the number of times the aileron exceeded 1.5^{o} in magnitude is plotted in Figures 33 and 34 versus the Dutch Roll handling qualities. In this case, this measure of pilot activity is directly related to handling qualities and the region are complimentary; that is, pilot opinion of a configuration is worse when more aileron activity is required.

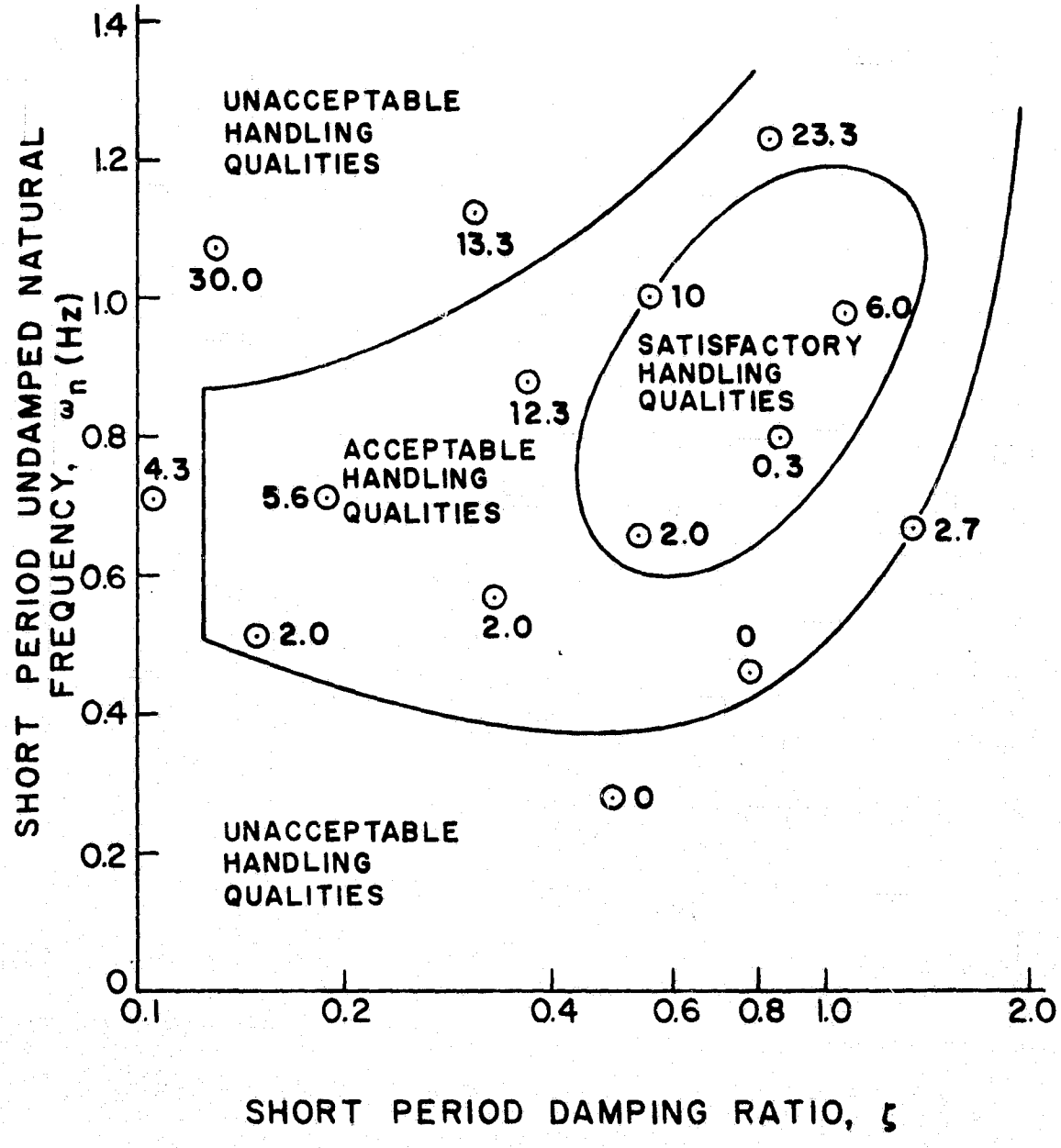

FIGURE 32. ELEVATOR ACTIVITY, SHORT-PERIOD HANDLING QUALITIES

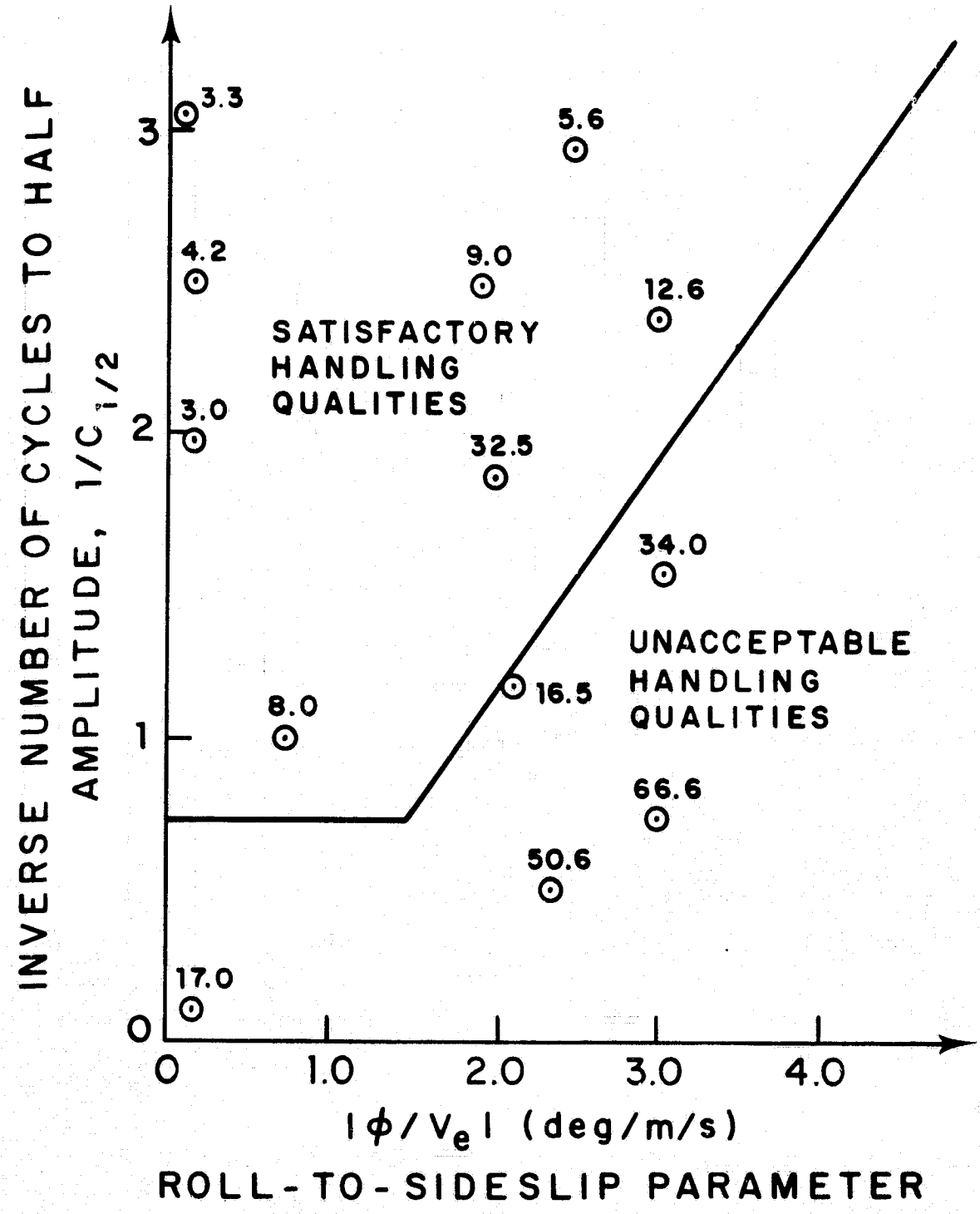

FIGURE 33. AILERON ACTIVITY, DUTCH ROLL HANDLING QUALITIES
($1/C_{i_{\frac{1}{2}}}$ vs. $|\phi/v_e|$)

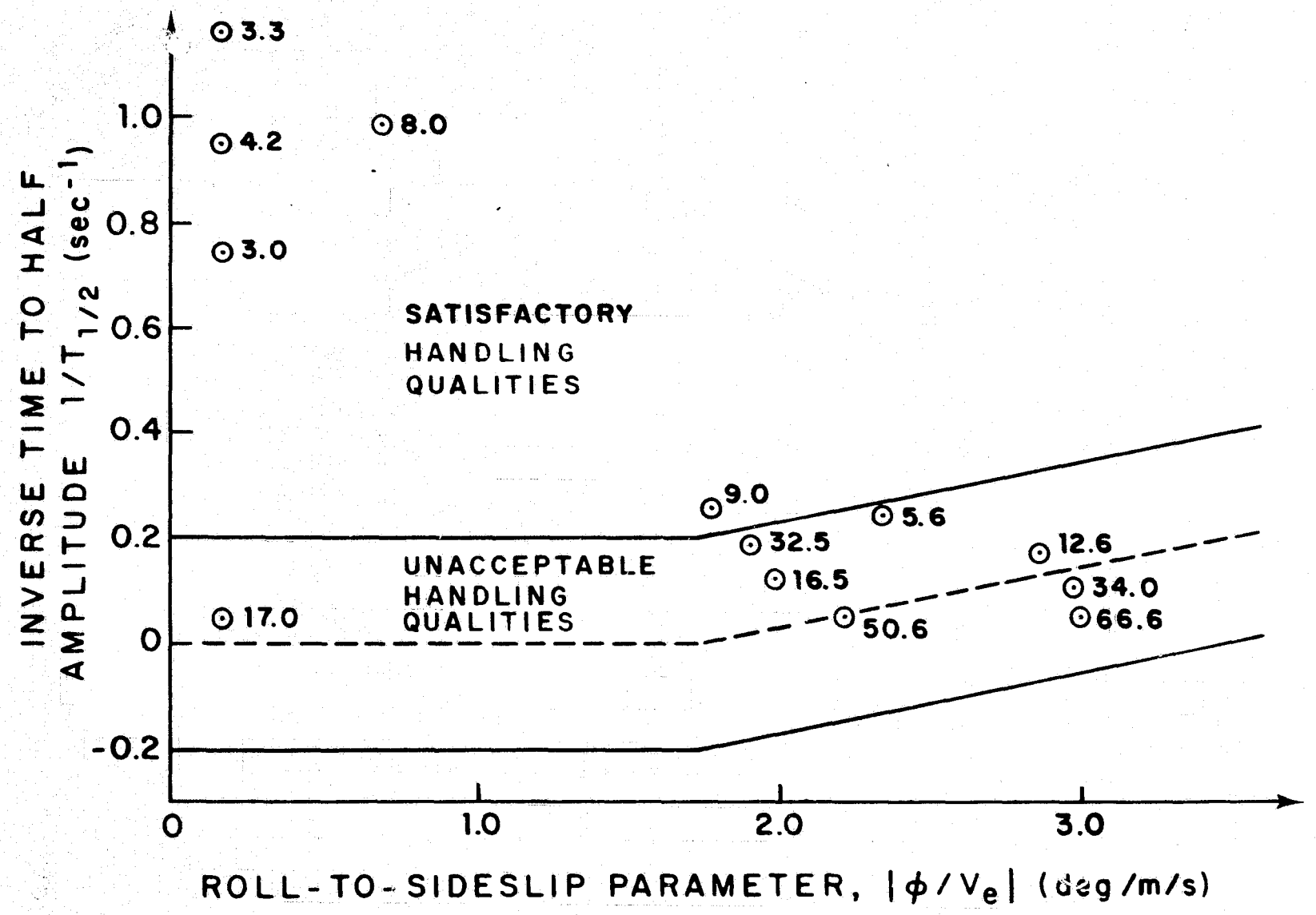

FIGURE 34. AILERON ACTIVITY, DUTCH ROLL HANDLING QUALITIES, ($1/T_{\frac{1}{2}}$ vs. $|\phi/v_e|$)

CHAPTER V

SUMMARY AND RECOMMENDATIONS

The interaction between ride and handling qualities for a typical STOL aircraft has been investigated. Simultaneous measurements of ride and handling qualities were made using a motion-based aircraft simulator and varying the short-period and Dutch Roll characteristics of the basic design. After plotting the ride quality associated with each test configuration along with the present requirements for short-period and Dutch Roll handling qualities, several important trends have been found. There appears to be a distinct trade-off between longitudinal short-period handling qualities and ride quality. Good Dutch Roll handling qualities and ride quality seem to be somewhat complimentary, but are, nevertheless, strongly related. It is up to the designers of future aircraft, particularly low-wing loading aircraft, to be aware of a vehicle's ride qualities as well as its handling qualities, and the results presented here should begin to guide him in these areas.

Future work is recommended to investigate these interrelationships in a much more comprehensive manner. More test cases should be chosen to obtain measurements to better define how ride qualities vary as handling qualities are varied over their acceptable regions. Other stability derivatives than the ones used in this study could be chosen to vary the short-period and Dutch Roll handling characteristics to determine if individual derivatives have unique effects on

the levels of ride quality measured. This is particularly important to investigate for the lateral Dutch Roll mode.

Likewise, the effects of variations in wing loading, turbulence level and power spectra, and flight conditions should be determined by repeating the tests as these additional parameters are changed. Ultimately, a general relationship could be developed to define the levels of ride quality to be expected of a given configuration as a function of all the above parameters.

APPENDIX A

UNIVERSITY OF VIRGINIA ANALOG FLIGHT SIMULATOR

The simulator used in the preliminary studies consists of a fixed-base cockpit with rudder, stick, and throttle controls. The cockpit instrumentation includes artificial horizon, altimeter, rate of climb indicator, airspeed indicator, heading indicator (compass), and glide slope and localizer indications (ILS). The cockpit is connected to two analog computers, an EAI-580 and Pace TR-20, programmed with the six-degree-of-freedom equations of motion, ILS equations, and equations to compute the sum-of-squares of the lateral and vertical accelerations. A photograph of the instrumentation and the entire apparatus is presented as Figure 1 in the text. A more thorough description of the equipment may be found in references (25) and (26).

APPENDIX B

DERIVATION OF ANALOG EQUATIONS OF MOTION

The six-degree-of-freedom equations of motion in Eulerian axes for a rigid body with an x-z plane of mirror symmetry are as follows (27):

$$\dot{U} + QW - RV + g \sin \Theta = \Sigma X/m = a_x$$

$$\dot{V} + RU - PW - g \sin \Phi \cos \Theta = \Sigma Y/m = a_y$$

$$\dot{W} + PV - QU - g \cos \Phi \cos \Theta = \Sigma Z/m = a_z$$

$$\dot{P} - (R + PQ) \frac{I_{xz}}{I_x} + RQ \left(\frac{I_z - I_y}{I_x}\right) = \frac{\Sigma L}{I_x}$$

$$\dot{Q} + (P^2 - R^2) \frac{I_{xz}}{I_y} + PR \left(\frac{I_x - I_z}{I_y}\right) = \frac{\Sigma M}{I_y}$$

$$\dot{R} + (QR - P) \frac{I_{xz}}{I_z} + QP \left(\frac{I_y - I_x}{I_z}\right) = \frac{\Sigma N}{I_z}$$

Using the standard perturbation technique (24), the following nondimensional equations are obtained:

$$C_{x_u} Sq'_\infty u + C_{x_\alpha} Sq_\infty \alpha + \frac{\bar{c}}{2U_0} C_{x_q} Sq_\infty \dot{\theta} + \frac{\bar{c}}{2U_0} C_{x_{\dot{\alpha}}} Sq_\infty \dot{\alpha} + C_{x_{\delta_e}} Sq_\infty \delta_e$$

$$+ C_{x_{\delta_T}} Sq_\infty \delta_T = mg\theta + mU_0[\ddot{u}' + \dot{\theta}\alpha - \dot{\psi}\beta]$$

$$C_{y_\beta} Sq_\infty \beta + \frac{b}{2U_0} C_{y_p} Sq_\infty \dot{\phi} + \frac{b}{2U_0} C_{y_r} Sq_\infty \dot{\psi} + C_{y_{\delta_r}} Sq_\infty \delta_r + C_{y_{\delta_a}} Sq_\infty \delta_a$$

$$+ C_{y_\phi} Sq_\infty \phi = mU_0[\dot{\beta} + \dot{\psi}' u - \dot{\phi}\alpha + \dot{\psi}]$$

$$C_{z_u} Sq_\infty {}'u + C_{z_\alpha} Sq_\infty \alpha + \frac{\bar{c}}{2U_0} C_{z_q} Sq_\infty \dot{\theta} + \frac{\bar{c}}{2U_0} C_{z_{\dot{\alpha}}} Sq_\infty \dot{\alpha} + C_{z_{\delta_e}} Sq_\infty \delta_e$$

$$+ C_{z_{\delta_T}} Sq_\infty \delta_T = mU_0[\dot{\alpha} + \dot{\phi}\beta - \dot{\theta}\,{}'u - \dot{\theta}]$$

$$C_{\ell_\beta} bSq_\infty \beta + \frac{b}{2U_0} C_{\ell_p} bSq_\infty \dot{\phi} + \frac{b}{2U_0} C_{\ell_r} bSq_\infty \dot{\psi} + C_{\ell_{\delta_r}} bSq_\infty \delta_r$$

$$+ C_{\ell_{\delta_a}} bSq_\infty \delta_a = \ddot{\phi} I_x - (\ddot{\psi} + \dot{\phi}\dot{\theta}) I_{xz} + \dot{\theta}\dot{\psi}(I_z - I_y)$$

$$C_{m_u} \bar{c}Sq_\infty {}'u + C_{m_\alpha} \bar{c}Sq_\infty \alpha + \frac{\bar{c}}{2U_0} C_{m_q} \bar{c}Sq_\infty \dot{\theta} + \frac{\bar{c}}{2U_0} C_{m_{\dot{\alpha}}} \bar{c}Sq_\infty \dot{\alpha} + C_{m_{\delta_e}} \bar{c}Sq_\infty \delta_e$$

$$+ C_{m_{\delta_T}} \bar{c}Sq_\infty \delta_T = \ddot{\theta} I_y + (\ddot{\phi}^2 - \ddot{\psi}^2) I_{xz} + \dot{\phi}\dot{\psi}(I_x - I_z)$$

$$C_{n_\beta} bSq_\infty \beta + \frac{b}{2U_0} C_{n_p} bSq_\infty \dot{\phi} + \frac{b}{2U_0} C_{n_r} bSq_\infty \dot{\psi} + C_{n_{\delta_r}} bSq_\infty \delta_r$$

$$+ C_{n_{\delta_a}} bSq_\infty \delta_a = \ddot{\psi} I_z + (\dot{\theta}\dot{\psi} - \ddot{\phi}) I_{xy} + \dot{\phi}\dot{\theta}(I_y - I_z) \,.$$

These are rearranged for ease in analog programming. An order of magnitude analysis allows the products of inertia and differences in moments of inertia terms to be neglected compared to other terms in the moment equations, yielding

$$-{}'\dot{u} = -\dot{\psi}\beta + \dot{\theta}\alpha - \frac{C_{x_u} Sq_\infty}{mU_0} {}'u - \frac{C_{x_{\dot{\alpha}}} \bar{c}Sq_\infty}{2mU_0^2} \dot{\alpha} - \frac{C_{x_\alpha} Sq_\infty}{mU_0} \alpha$$

$$- \frac{C_{x_q} \bar{c}Sq_\infty}{2mU_0^2} \dot{\theta} + \frac{g}{U_0} \theta - \frac{C_{x_{\delta_e}} Sq_\infty}{mU_0} \delta_e - \frac{C_{x_{\delta_T}} Sq_\infty}{mU_0} \delta_T$$

$$-\dot{\beta} = -\dot{\phi}\alpha + \dot{\psi}'u + \dot{\psi} - \frac{C_{y_r} bSq_\infty}{2mU_0^2}\dot{\psi} - \frac{C_{y_\beta} Sq_\infty}{mU_0}\beta - \frac{C_{y_{\delta_r}} Sq_\infty}{mU_0}\delta_r$$
$$- \frac{C_{y_{\delta_a}} Sq_\infty}{mU_0}\delta_a - \frac{C_{y_p} bSq_\infty}{2mU_0^2}\dot{\phi} - \frac{C_{y_\phi} Sq_\infty}{mU_0}\phi$$

$$-\dot{\alpha} = \frac{mU_0/Sq_\infty + \bar{c}/2U_0 C_{z_q}}{mU_0/Sq_\infty - \bar{c}/2U_0 C_{z_{\dot{\alpha}}}}\dot{\theta} - \frac{mU_0/Sq_\infty}{mU_0/Sq_\infty - \bar{c}/2U_0 C_{z_{\dot{\alpha}}}}\dot{\theta}'u$$
$$+ \frac{mU_0/Sq_\infty}{mU_0/Sq_\infty - \bar{c}/2U_0 C_{z_{\dot{\alpha}}}} - \frac{C_{z_u}}{mU_0/Sq_\infty - \bar{c}/2U_0 C_{z_{\dot{\alpha}}}}'u$$
$$- \frac{C_{z_\alpha}}{mU_0/Sq_\infty - \bar{c}/2U_0 C_{z_{\dot{\alpha}}}}\alpha - \frac{C_{z_{\delta_e}}}{mU_0/Sq_\infty - \bar{c}/2U_0 C_{z_{\dot{\alpha}}}}$$
$$- \frac{C_{z_{\delta_T}}}{mU_0/Sq_\infty - \bar{c}/2U_0 C_{z_{\dot{\alpha}}}}\delta_T$$

$$-\dot{\phi} = -\frac{C_{\ell_\beta} bSq_\infty}{I_x}\beta - \frac{C_{\ell_p} b^2 Sq_\infty}{2U_0 I_x}\dot{\phi} - \frac{C_{\ell_r} b^2 Sq_\infty}{2U_0 I_x}\dot{\psi}$$
$$- \frac{C_{\ell_{\delta_r}} bSq_\infty}{I_x}\delta_r - \frac{C_{\ell_{\delta_a}} bSq_\infty}{I_x}\delta_a$$

$$-\ddot{\theta} = -\frac{C_{m_u} \bar{c}Sq_\infty}{I_y}'u - \frac{C_{m_\alpha} \bar{c}Sq_\infty}{I_y}\alpha - \frac{C_{m_q} \bar{c}^2 Sq_\infty}{2U_0 I_y}\dot{\theta}$$
$$- \frac{C_{m_{\dot{\alpha}}} \bar{c}^2 Sq_\infty}{2U_0 I_y}\dot{\alpha} - \frac{C_{m_{\delta_e}} \bar{c}Sq_\infty}{I_y}\delta_e - \frac{C_{m_{\delta_T}} \bar{c}Sq_\infty}{I_y}\delta_T$$

$$-\ddot{\psi} = -\frac{C_{n_\beta} bSq_\infty}{I_z}\beta - \frac{C_{n_p} b^2 Sq_\infty}{2U_0 I_z}\dot{\phi} - \frac{C_{n_r} b^2 Sq_\infty}{2U_0 I_z}\dot{\psi}$$
$$- \frac{C_{n_{\delta_r}} bSq_\infty}{I_z}\delta_r - \frac{C_{n_{\delta_a}} bSq_\infty}{I_z}\delta_a .$$

APPENDIX C

DEFINITION OF STABILITY DERIVATIVES

Longitudinal Equations

$$C_L = \frac{W}{q_\infty S}$$

$$C_{D_\alpha} = \frac{\partial C_D}{\partial \alpha}$$

$$C_D = \frac{D}{q_\infty S}$$

$$C_{D_u} = \frac{\partial C_D}{\partial (u/U_0)}$$

$$C_{D_{\delta_e}} = \frac{\partial C_D}{\partial \delta_e}$$

$$C_{L_\alpha} = \frac{\partial C_L}{\partial \alpha}$$

$$C_{L_{\dot\alpha}} = \frac{\partial C_L}{\partial (\dot\alpha \bar{c}/2U_0)}$$

$$C_{L_u} = \frac{\partial C_L}{\partial (u/U_0)}$$

$$C_{L_q} = \frac{\partial C_L}{\partial (q\ \bar{c}/2U_0)}$$

$$C_{L_{\delta_e}} = \frac{\partial C_L}{\partial \delta_e}$$

$$C_{m_\alpha} = \frac{\partial C_m}{\partial \alpha}$$

$$C_{m_{\dot\alpha}} = \frac{\partial C_m}{\partial (\dot\alpha \bar{c}/2U_0)}$$

$$C_{m_u} = \frac{\partial C_m}{\partial (u/U_0)}$$

$$C_{m_q} = \frac{\partial C_m}{\partial (q\ \bar{c}/2U_0)}$$

$$C_{m_{\delta_e}} = \frac{\partial C_m}{\partial \delta_e}$$

$$C_{x_u} = -C_{D_u} - 2C_D$$

$$C_{z_u} = -C_{L_u} - 2C_L$$

$$C_{x_\alpha} = C_L - C_{D_\alpha}$$

$$C_{z_\alpha} = -C_{L_\alpha} - C_D$$

$$C_{x_{\dot\alpha}} = -C_{D_{\dot\alpha}}$$

$$C_{z_{\dot\alpha}} = -C_{L_{\dot\alpha}}$$

$$C_{x_q} = -C_{D_q}$$

$$C_{z_q} = -C_{L_q}$$

Lateral-directional Equations

$$C_{y_\beta} = \frac{\partial C_y}{\partial \beta}$$

$$C_{y_p} = \frac{\partial C_y}{\partial (pb/2U_0)}$$

$$C_{y_r} = \frac{\partial C_y}{\partial (rb/2U_0)}$$

$$C_{y_\phi} = \frac{\partial C_y}{\partial \phi}$$

$$C_{y_{\delta_r}} = \frac{\partial C_y}{\partial \delta_r}$$

$$C_{y_{\delta_a}} = \frac{\partial C_y}{\partial \delta_a}$$

$$C_{\ell_\beta} = \frac{\partial C_\ell}{\partial \beta}$$

$$C_{\ell_p} = \frac{\partial C_\ell}{\partial (pb/2U_0)}$$

$$C_{\ell_r} = \frac{\partial C_\ell}{\partial (rb/2U_0)}$$

$$C_{\ell_{\delta_r}} = \frac{\partial C_\ell}{\partial \delta_r}$$

$$C_{\ell_{\delta_a}} = \frac{\partial C_\ell}{\partial \delta_a}$$

$$C_{n_\beta} = \frac{\partial C_n}{\partial \beta}$$

$$C_{n_p} = \frac{\partial C_n}{\partial (pb/2U_0)}$$

$$C_{n_r} = \frac{\partial C_n}{\partial (rb/2U_0)}$$

$$C_{n_{\delta_r}} = \frac{\partial C_n}{\partial \delta_r}$$

$$C_{n_{\delta_a}} = \frac{\partial C_n}{\partial \delta_a}$$

APPENDIX D

SIGN CONVENTIONS

Sign conventions for forces, moments, angular rates, and linear velocities are shown in the sketch below. The positive sense of each variable is shown.

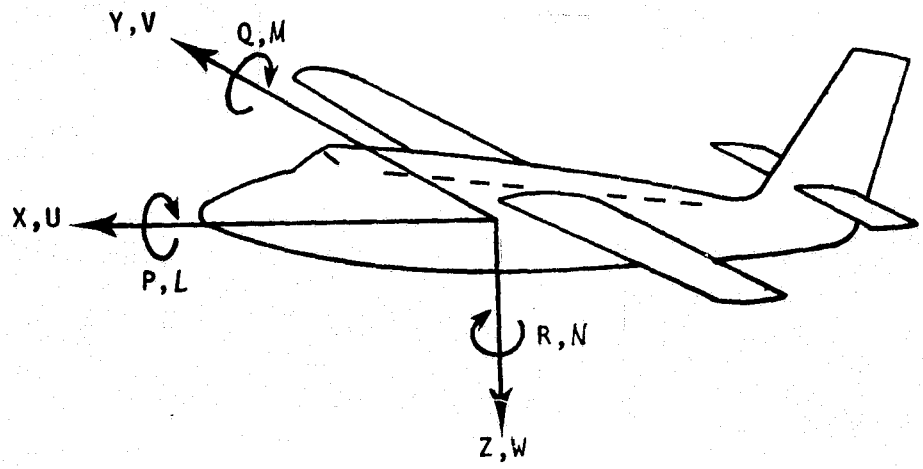

(Reference 14)

Sign conventions for control deflections are listed below:

Control Surface	Positive Deflection
Elevator	Trailing edge down
Ailerons	Left aileron trailing edge down Right aileron trailing edge up
Rudder	Trailing edge left

APPENDIX E

DERIVATION OF EXPRESSION FOR NORMAL ACCELERATION DUE TO TURBULENCE

If one eliminates the force equation in the X body axis direction, assumes variations in u to be negligible, neglects C_{z_q} and $C_{z_{\dot{\alpha}}}$ and assumes a sinusoidal forcing function, the following equations result (24):

$$(2\mu s - C_{z_\alpha})\alpha - (2\mu)q = (-C_{z_\alpha})\frac{\bar{w}_g}{U_0}$$

$$-(C_{m_{\dot{\alpha}}}s + C_{m_\alpha})\alpha + (i_B s - C_{m_q})q = (-C_{m_\alpha} - C_{m_{\dot{\alpha}}}s + sC_{m_q})\frac{\bar{w}_g}{U_0}$$

where $\mu = m/\rho S\ell$

$i_B = I_y/\rho S\ell^3$

$\ell = \bar{c}/2$

s = Laplace operator

$\bar{w}_g$ = gust input magnitude.

One may solve these expressions for $\alpha/\bar{w}_g$ and $q/\bar{w}_g$ by Cramer's rule to find

$$\frac{\alpha}{\bar{w}_g} = \frac{1}{U_0\Delta}\left[(-C_{m_\alpha} - C_{m_{\dot{\alpha}}}s + C_{m_q}s)(2\mu) - C_{z_\alpha}(i_B s - C_{m_q})\right]$$

$$\frac{q}{\bar{w}_g} = \frac{1}{U_0\Delta}\left[(2\mu s - C_{z_\alpha})(-C_{m_\alpha} - C_{m_{\dot{\alpha}}}s + C_{m_q}s) - C_{z_\alpha}(C_{m_{\dot{\alpha}}}sC_{m_\alpha})\right]$$

$$\Delta = (2\mu s - C_{z_\alpha})(i_B s - C_{m_q}) - 2\mu(C_{m_{\dot{\alpha}}} s + C_{m_\alpha}) \quad .$$

The transfer function for the acceleration factor is given by

$$\frac{n}{\bar{w}_g} = \frac{2U_0^2}{g\bar{c}} \left(\frac{q}{\bar{w}_g} - s\,\frac{\alpha}{\bar{w}_g}\right) \quad .$$

Making the substitutions for $q/\bar{w}_g$ and $\alpha/\bar{w}_g$, the following expression results:

$$\frac{n}{\bar{w}_g} = \frac{2U_0}{g\bar{c}\Delta} \left(-2C_{m_q} C_{z_\alpha}\right) s \quad .$$

Setting $s = i\omega$, one may form the expression:

$$\left|\frac{n}{\bar{w}_g}\right|^2 = \frac{4U_0^2}{g^2\bar{c}^2} \frac{4C_{m_q}^2 C_{z_\alpha}^2 \omega^2}{[(-2\mu C_{m_q} - i_B C_{z_\alpha} - 2\mu C_{m_{\dot{\alpha}}})^2\omega^2 + (C_{z_\alpha} C_{m_q} - 2\mu C_{m_\alpha} - 2\mu i_B \omega^2)^2]} \quad .$$

As a measure of the total normal acceleration, we will form

$$a_N = \int_{-\infty}^{\infty} \left|\frac{n}{\bar{w}_g}\right|^2 d\omega \quad .$$

This may now be written as:

$$a_N = K \int_{-\infty}^{\infty} \frac{\omega^2 d\omega}{A + B\omega^2 + \omega^4}$$

where $A = \left(\dfrac{C_{z_\alpha} C_{m_q} - 2\mu C_{m_\alpha}}{2\mu i_B}\right)^2$ and

$$B = \frac{(-2\mu C_{m_q} - i_B C_{z_\alpha} - 2\mu C_{m_{\dot{\alpha}}})^2 - 4\mu i_B (C_{z_\alpha} C_{m_q} - 2\mu C_{m_\alpha})}{4\mu^2 i_B{}^2} .$$

Following the development in Reference (24) for an approximation of the short-period mode, the following relations are obtained for ω_{n_s} and ζ_s

$$\omega_{n_s}{}^2 = \frac{C_{z_\alpha} C_{m_q} - 2\mu C_{m_\alpha}}{2\mu i_B}$$

$$2\zeta_s \omega_{n_s} = - \frac{2\mu C_{m_q} + i_B C_{z_\alpha} + 2\mu C_{m_{\dot{\alpha}}}}{2\mu i_B} .$$

By use of the two previous expressions for $\omega_{n_s}{}^2$ and $2\zeta_s\omega_{n_s}$, it can be seen that

$$A = \omega_{n_s}{}^4 \qquad \text{and}$$

$$B = 2\omega_{n_s}{}^2(2\zeta_s{}^2 - 1) .$$

Solving

$$\int_{-\infty}^{\infty} \frac{\omega^2 d\omega}{A + B\omega^2 + \omega^4}$$

we attempt to write this in the form

$$\int_{-\infty}^{\infty} \frac{\omega^2 d\omega}{(E + \omega^2)(F + \omega^2)}$$

where $$E,F = \frac{B \pm \sqrt{B^2 - 4A}}{2} .$$

We now examine the quantity $B^2 - 4A$:

$$B^2 - 4A = [2\omega_{n_s}{}^2(2\zeta_s{}^2 - 1)]^2 - 4\omega_{n_s}{}^4 = 4\omega_{n_s}{}^4\zeta_s{}^2(\zeta_s{}^2 - 1) \ .$$

From this, we may identify three different cases for the roots of the characteristic denominator.

Case 1. $\zeta_s{}^2 < 1$

Complex roots exist since $B^2 - 4A < 0$. Integrating

$$\int_{-\infty}^{\infty} \frac{\omega^2 d\omega}{A + B\omega^2 + \omega^4}$$

over the complex plane, we obtain the following result after much complex arithmetic

$$\int_{-\infty}^{\infty} \frac{\omega^2 d\omega}{A + B\omega^2 + \omega^4} = \frac{\pi}{2\omega_{n_s}\sqrt{1 - \zeta^2}} \ .$$

Case 2. $\zeta_s{}^2 = 1$

Two real equal roots exist since $B^2 - 4A = 0$. Integrating, we find

$$\int_{-\infty}^{\infty} \frac{\omega^2 d\omega}{A + B\omega^2 + \omega^4} = \frac{\pi}{2\omega_{n_s}} \ .$$

Case 3. $\zeta_s{}^2 > 1$

Two real unequal roots exist since $B^2 - 4A > 0$. Again, integrating we find

$$\int_{-\infty}^{\infty} \frac{\omega^2 d\omega}{A + B\omega^2 + \omega^4} = \frac{\pi(E\sqrt{F} - F\sqrt{E})}{\sqrt{EF}\,(E - F)}$$

$$= \frac{\pi[2\zeta_s^2 - 1 + 2\zeta_s\sqrt{\zeta_s^2 - 1}][2\zeta_s^2 - 1 - 2\zeta_s\sqrt{\zeta_s^2 - 1}]^{\frac{1}{2}}}{4\omega_{n_s}\zeta_s\sqrt{\zeta_s^2 - 1}}$$

$$- \frac{[2\zeta_s^2 - 1 - 2\zeta_s\sqrt{\zeta_s^2 - 1}][2\zeta_s^2 - 1 + 2\zeta_s\sqrt{\zeta_s^2 - 1}]^{\frac{1}{2}}}{4\omega_{n_s}\zeta_s\sqrt{\zeta_s^2 - 1}} .$$

If one plots the numerator function over the range $1.1 < \zeta_s < 2.0$, one finds it nearly linear in ζ_s. We may then write

$$\int_{-\infty}^{\infty} \frac{\omega^2 d\omega}{A + B\omega^2 + \omega^4} \doteq \frac{K\pi}{4\omega_{n_s}\sqrt{\zeta_s^2 - 1}} .$$

In the original expression for a_N, a constant K appeared which was a function of the product $C_{z_\alpha}{}^2 C_{m_q}{}^2$. In this study C_{z_α} is held fixed and C_{m_q} is used as a variable to modify the short-period characteristics. An examination of test cases 1, 2, and 13 ($C_{m_\alpha} = 1.9098$) reveals that there is almost a linear relationship between C_{m_q} and ζ_s. A mathematical fit to this trend is $\zeta_s = -0.011\, C_{m_q} + 0.332$ or $C_{m_q} \approx 33(1 - 3\zeta_s)$. Incorporating this function into the three expressions gives

$$a_N = K_1 \frac{\bar{w}_g (1 - 3\zeta_s)^2}{\omega_{n_s} \sqrt{1 - \zeta_s^2}} \qquad \zeta_s < 1$$

$$a_N = K_2 \frac{\bar{w}_g}{\omega_{n_s}} \qquad \zeta_s = 1$$

$$a_N = K_3 \frac{\bar{w}_g (1 - 3\zeta_s)^2}{\omega_{n_s} \sqrt{\zeta_s^2 - 1}} \qquad \zeta_s > 1.$$

where the constants K_1, K_2, and K_3 are functions of flight conditions, aircraft mass, pitch moment of inertia, and the stability derivative C_{z_α}.

Expanding the radicals by the binomial expansions yields

$$(1/\sqrt{1 - \zeta_s^2}) = 1 - \frac{1}{2}\zeta^2 + \frac{3}{8}\zeta^4 + \text{H.O.T.}$$

$$(1/\sqrt{\zeta^2 - 1}) = 1/\zeta - \frac{1}{2}\frac{1}{\zeta^3} + \frac{3}{8}\frac{1}{\zeta^5} + \text{H.O.T.}$$

Thus

$$\frac{(1 - 3\zeta_s)^2}{\sqrt{1 - \zeta_s^2}} = 1 - 6\zeta_s + 8.5\zeta_s^2 + \text{H.O.T.} \qquad \zeta_s < 1$$

$$\frac{(1 - 3\zeta_s)^2}{\sqrt{\zeta_s^2 - 1}} = 9\zeta_s - 6 - \frac{7}{2\zeta} + \text{H.O.T.} \qquad \zeta_s > 1$$

and simplified expressions for a_N are

$$a_N = K_1 \frac{\bar{w}_g}{\omega_{n_s}} (1 - 6\zeta_s + 8.5\zeta_s^2 + \text{H.O.T.}) \qquad \zeta_s < 1$$

$$a_N = K_2 \frac{\bar{w}_g}{\omega_{n_s}} \qquad \zeta_s = 1$$

$$a_N = K_3 \frac{\bar{w}_g}{n_s} (9\zeta_s - 6 - \frac{7}{2\zeta_s} + \text{H.O.T.}) \qquad \zeta_s > 1.$$

It should be noted here that the mathematical fit for C_{m_q} versus ζ_s is unique to the particular value of C_{m_α} chosen. However, fits for other values of C_{m_α} = constant exhibited the same trends as above, that is $C_{m_q} \approx (1 - k\zeta_s)$ where k is a positive constant. Therefore, in general

$$a_N = K_1 \frac{\bar{w}_g (1 - k\zeta_s)^2}{\omega_{n_s} \sqrt{1 - \zeta_s^2}} \qquad \zeta_s < 1$$

$$a_N = K_2 \frac{\bar{w}_g}{\omega_{n_s}} \qquad \zeta_s = 1$$

$$a_N = K_3 \frac{\bar{w}_g (1 - k\zeta_s)^2}{\omega_{n_s} \sqrt{\zeta_s^2 - 1}} \qquad \zeta_s > 1.$$

REFERENCES

1. Anonymous, "Flying Qualities of Piloted Airplanes," Military Specification MIL-F-8785(ASG), September 1954.

2. Anonymous, "Flying Qualities of Piloted Airplanes," Military Specification MIL-F-8785B(ASG), August 1969.

3. Anonymous, "Flying Qualities of Piloted V/STOL Airplanes," Military Specification MIL-F-83300, December 1970.

4. Newell, F. and Campbell, G., "Flight Evaluations of Variable Short Period and Phugoid in a B-26," Cornell Aeronautical Laboratory (CAL) Report TB-757-F-11, 1954.

5. Bull, G., "A Flight Investigation of Acceptable Roll to Yaw Ratio of the Dutch Roll and Acceptable Spiral Divergence," Cornell Aeronautical Laboratory (CAL) Report TB-574-F-6, 1952.

6. O'Hara, F., "Handling Criteria," J. Royal Aeronautical Society, Vol. 71, No. 676, pp. 271-291, 1967.

7. Flight Standards Service, "Tentative Airworthiness Standards for Powered Lift Transport Category Aircraft," Federal Aviation Administration, Department of Transportation, August 1970.

8. Advisory Group for Aeronautical Research and Development, "Recommendations for V/STOL Handling Qualities," North Atlantic Treaty Organization Report 408A, October 1964.

9. Stone, Ralph W., Jr., "Ride-Quality Overview," Symposium on Vehicle Ride Quality, NASA Langley Research Center, Hampton, Virginia, July 6-7, 1972, NASA Technical Memorandum NASA TM X-2620, October 1972.

10. Eastern Air Lines and McDonnell Aircraft Company, "STOL Demonstration Program," EAL Flight A&D 68-315, MDC-G-984, March 1969.

11. International Standards Organization Technical Committee 108 Working Group 7, "Guide for the Evaluation of Human Exposure to Whole Body Vibration, Mechanical Vibration and Shock," March 1970.

12. Jacobson, I. D., "Environmental Criteria for Human Comfort--A Study of Related Literature," NASA Contractor Report NASA CR-132424, February 1974.

13. Rudrapatna, Ashok N., "Modelling of Aircraft Ride Quality," Master's Thesis, University of Virginia, Charlottesville, June 1973.

C-2

14. Gordon, C. K. and Dodson, R. O., "STOL Ride Control Feasibility Study," The Boeing Company, NASA Contractor Report NASA CR-2276, July 1973.

15. Blakelock, John H., Automatic Control of Aircraft and Missiles, John Wiley and Sons, Inc., New York, 1965.

16. Kuhlthau, A. R. and Jacobson, I. D., "Analysis of Passenger Acceptance of Commercial Flights Having Characteristics Similar to STOL," University of Virginia, STOL Program Technical Report 403208, March 1973.

17. Richards, L. G. and Jacobson, I. D., "Ride Quality Evaluation I: Questionnaire Studies of Airline Passenger Comfort," Ergonomics, Vol. 18, No. 2, pp. 129-150, March 1975.

18. Parrish, Russell V., Dieudonne, James E. and Martin, Dennis J., Jr., "Motion Software for a Synergistic Six-Degree-of-Freedom Motion Base," NASA Langley Research Center, NASA Technical Note NASA TN D-7350, December 1973.

19. Parrish, Russell V., Dieudonne, James E., Martin, Dennis J., Jr. and Copeland, James L., "Compensation Based on Linearized Analysis for a Six-Degree-of-Freedom Motion Simulator," NASA Langley Research Center, NASA Technical Note NASA TN D-7349, November 1973.

20. Dieudonne, James E., Parrish, Russell V. and Bardusch, Richard E., "An Actuator Extension Transformation for a Motion Simulator and an Inverse Transformation Applying Newton-Raphson's Method," NASA Langley Research Center, NASA Technical Note NASA TN D-7067, November 1972.

21. Cooper, G. E. and Harper, R. P., Jr., "The Use of Pilot Rating in the Evaluation of Aircraft Handling Qualities," NASA Technical Note NASA TN D-5153, April 1969.

22. Jacobson, I. D. and Kuhlthau, A. R., "Mathematical Modeling to Determine Criteria for Evaluating Human Acceptance of Transportation Systems," University of Virginia, STOL Program Technical Report 403206, August 1972.

23. Jacobson, I. D. and Kuhlthau, A. R., "Flight Research Experiments to Determine Ride Quality and Passenger Acceptance," University of Virginia, STOL Program Status Report 403903 (unpublished data), July 1974.

24. Etkin, Bernard, Dynamics of Flight, John Wiley and Sons, Inc., New York, 1959.

25. Buckley, James E., "An Evaluation of the University of Virginia Aircraft Cockpit Simulator," Bachelor of Science Thesis, University of Virginia, December 1973.

26. McDaniel, James C., Jr., "The Development of a Six-Degree-of-Freedom Aircraft Simulator," Bachelor of Science Thesis, University of Virginia, June 1971.

27. Kolk, W. Richard, Modern Flight Dynamics, Prentice-Hall, Inc. Englewood Cliffs, New Jersey, 1961.